Mouse genetic analyses of Spir functions

This thesis is submitted to obtain the academic degree of
Doctor rerum naturalium (Dr. rer. nat.)
from the Julius-Maximilians-University of Würzburg

submitted by

Sandra Pleiser
born in Engelskirchen

Würzburg 2012

Eingereicht am:

Mitglieder der Promotionskommission:

Vorsitzender:
Gutachter: Prof. Dr. Eugen Kerkhoff
Gutachter: Prof. Dr. Thomas Raabe

Tag des Promotionskolloquiums:

Doktorurkunde ausgehändigt am:

Erklärung

Hiermit erkläre ich, dass ich die Dissertation ”Mouse genetic analyses of Spir functions” selbstständig angefertigt habe und keine anderen als die von mir angegebenen Hilfsmittel und Quellen verwendet habe.

Ich erkläre außerdem, dass diese Dissertation weder in gleicher noch in anderer Form bereits in einem anderen Prüfungsverfahren vorgelegen hat.

Ich habe früher, außer den mit dem Zulassungsgesuch urkundlich vorgelegten Graden, keine weiteren akademischen Grade erworben oder zu erwerben versucht.

Würzburg,

Sandra Pleiser

Summary

The actin cytoskeleton is essential for many cellular functions, such as the regulation of cell morphology, cell migration and vesicle transport processes. The functional diversity of actin structures is reflected in a variety of distinct molecular mechanisms regulating the polymerization of actin filaments. The spontaneous polymerization of actin however is inhibited, by both the instability of small actin oligomers and by actin monomer binding proteins, which prevent the formation of such oligomers. Actin nucleation factors help to overcome this kinetic barrier of filament initiation and are essential for the generation of novel actin filaments at specified subcellular compartments.

Spir proteins are the founding members of the novel class of WH2 domain containing actin nucleation factors. They initiate actin polymerization by binding of actin monomers to four WH2 domains in the central part of the protein. Despite their ability to nucleate actin polymerization *in vitro* by themselves, Spir proteins form a regulatory complex with the distinct actin nucleators of the formin subgroup of formins. Spir functions in the regulation of vesicular originated filamentous actin structures, vesicle transport processes and the assembly of the cleavage furrow during asymmetric meiotic cell divisions. The mammalian genome encodes two *spir* genes, *spir-1* and *spir-2*. The corresponding proteins have an identical structural array and share a high degree of homology.

In order to elucidate the Spir function in developing and adult mouse tissues, the yet unknown expression of the mouse *spir-2* gene was addressed. Real-time PCR analysis revealed highest expression of *spir-2* in oocytes, the brain, throughout the gastrointestinal tract, testis and kidney of adult mice. *In situ* hybridizations were performed to substantiate the cellular nature of *spir* gene expression. During embryogenesis *in situ* hybridizations show *spir-2* to be expressed in the developing nervous system and intestine. In adult mouse tissues highest expression of *spir-2* was detected in the epithelial cells of the digestive tract, in neuronal cells of the nervous system and in spermatocytes. In contrast to the more restricted expression of the mouse *spir-1* gene, which is mainly found in the nervous system, oocytes and testis, the data presented here show a distinct and broader expression pattern of the *spir-2* gene and by this support a more general cell biological function of the novel actin nucleators.

In order to address the function of Spir proteins in the developing and adult nervous system, Spir-1 deficient mice were generated by a gene trap method. Spir-1 deficient mice are viable and provide a perfect tool to address the neurobiological function of the Spir-1 protein. Analyses of primary cortical neurons from Spir-1 deficient mice revealed a specific reduction of dendritic branchpoints and are the first description of

a neuronal Spir-1 function. Further, a transgenic mouse line (*thy1*-GFP-M) was employed that expresses the green fluorescent protein (GFP) under the control of neuron specific elements from the *thy1* promoter. GFP is thereby expressed in only a subset of neurons and labels the neurons in their entirety. Spir-1 deficient mice carrying the GFP transgene were generated and analyzed. It was found that Spir-1 deficient mice exhibit a reduced number of dendritic spines in the entorhinal cortex compared to wildtype littermates.

All together this study gives novel information about the cell biological function of Spir and provides insights how cytoskeletal functions structure the mammalian neuronal network.

Zusammenfassung

Das Aktin-Zytoskelett ist für viele zelluläre Funktionen unerlässlich, dazu gehören der strukturelle Aufbau von Zellen, die Zellwanderung und Vesikeltransportprozesse. Die funktionelle Vielfalt der Aktinstrukturen spiegelt sich in einer Vielzahl verschiedener molekularer Mechanismen wieder, welche die Polymerisierung von Aktinfilamenten regulieren. Die sponante Aktinpolymerisierung wird jedoch verhindert aufgrund der Instabilität von kleinen Aktin Oligomeren und durch Aktin Monomer bindende Proteine, welche die Bildung solcher Oligomere unterbinden. Aktinnukleationsfaktoren helfen diese kinetische Barriere der Filamentbildung zu überwinden und sind wesentlich für die Erzeugung von neuen Aktinfilamenten an bestimmten subzellulären Kompartimenten.

Spir Proteine sind die ersten beschriebenen Mitglieder der neuen Klasse von WH2 Domänen Aktinnukleationsfaktoren. Sie leiten die Polymerisierung von Aktin ein, indem sie Aktinmonomere an die vier WH2 Domänen im Zentrum des Proteins binden. Trotz ihrer Eigenschaft Aktinpolymerisation *in vitro* selber zu nukleieren, bilden Spir Proteine einen regulatorischen Komplex mit anderen Aktinnukleatoren der formin Untergruppe von forminen. Spir hat eine Funktion bei der Regulierung von vesikulär erzeugten filamentösen Aktinstrukturen, Vesikeltransportprozessen und der Bildung der Teilungsfurche während der asymmetrischen meiotischen Zellteilung. Das Säugetiergenom kodiert zwei *spir* Gene, *spir-1* und *spir-2*. Die entsprechenden Proteine haben einen identischen strukturellen Aufbau und sind zu einem großen Teil homolog zueinander.

Um die Spir Funktion im sich entwickelnden und adulten Nervensystem zu untersuchen, wurde die bisher unbekannte Expression des Maus *spir-2* Gens analysiert. Real-time PCR Analysen haben ergeben, dass *spir-2* in adulten Mäusen in Oozyten, dem Gehirn, im Gastrointestinaltrakt, den Hoden und der Niere exprimiert wird. *In situ* Hybridisierungen wurden durchgeführt um die zelluläre Natur der *spir* Expression nachzuweisen. Während der Embryogenese haben *in situ* Hybridisierungen gezeigt, dass *spir-2* im sich entwickelnden Nervensytem und Darmtrakt exprimiert wird. In adulten Mausgeweben, wurde die höchste Expression von *spir-2* in Epithelzellen des Verdauungstraktes, in neuronalen Zellen des Nervensystems und in Spermatocyten gefunden. Im Gegensatz zur eher begrenzten Expression des Maus *spir-1* Gens, welches überwiegend im Nervensystem, den Oozyten und Hoden zu finden ist, zeigen die hier aufgeführten Daten ein breiteres Expressionsmuster des *spir-2* Gens und unterstützen damit eine allgemeinere zellbiologische Funktion der neuen Aktinnukleatoren.

Um die Funktion des Spir Proteins im sich entwickelnden und adulten Nervensystem zu untersuchen, wurden Spir-1 defiziente Mäuse mit Hilfe der *gene trap* Methode

generiert. Spir-1 defiziente Mäuse sind lebensfähig und eignen sich daher perfekt um die Neurobiologie des Spir-1 Aktinnukleators zu untersuchen. Die Analyse von primären kortikalen Neuronen von Spir-1 defizienten Mäusen zeigte eine Reduktion dendritischer Verzweigungen und ist die erste Beschreibung einer neuronalen Funktion von Spir-1. Desweiteren wurde eine transgene Mauslinie (*thy1*-GFP-M) eingesetzt, die das grüne Fluoreszenzprotein (GFP) unter der Kontrolle von Neuronen-spezifischen Elementen des *thy1* Promoters exprimiert. GFP ist dabei nur in einer Teilmenge von Neuronen exprimiert, färbt diese Neuronen jedoch in ihrer Gesamtheit an. Spir-1 defiziente Mäuse, die das GFP Transgen exprimieren wurden generiert und analysiert. Es wurde herausgefunden, dass Spir-1 defiziente Mäuse eine reduzierte Anzahl an dendritischen Dornen im entorhinalen Kortex im Vergleich zu Wildtyp- Geschwistertieren aufweisen.
Zusammengefasst gibt diese Studie neue Erkenntnisse über die zellbiologische Funktion von Spir und liefert Einsichten wie das neuronale Netzwerk sturkturiert wird.

Table of contents

SUMMARY ..... **I**

ZUSAMMENFASSUNG ..... **III**

1 INTRODUCTION **1**

1.1 The actin cytoskeleton **1**

1.2 Actin nucleation **3**
1.2.1 Formins 4
1.2.2 The WH2 domain containing actin nucleation factor Spir 5
1.2.3 Spir/formin cooperation in actin nucleation 7

1.3 Spir function in vesicle transport processes **10**

1.4 Aim of the work **11**

2 RESULTS **12**

2.1 Tissue specific expression of the mouse *spir-1* and *spir-2* genes **12**
2.1.1 Relative mRNA expression of *spir-1* and *spir-2* 12
2.1.2 *spir-2* gene expression during mouse embryogenesis 14
2.1.3 Spatial *spir-2* gene expression in adult mouse tissues 17

2.2 Mouse genetic analyses **19**
2.2.1 Generation of Spir-1 deficient mice 19
2.2.2 Initial phenotyping of Spir-1 deficient mice 23
2.2.3 Spir-1 function in neuronal differentiation 24
2.2.3.1 Reduced number of dendritic branchpoints in Spir-1 deficient cultured primary cortical neurons 24
2.2.3.2 Impaired dendritic spine formation in Spir-1 deficient neurons 26

3 DISCUSSION **28**

3.1 Expression patterns of mammalian *spir* genes **28**
3.1.1 *spir-2* shows a broader expression pattern than *spir-1* 28
3.1.2 *spir* expression in the mouse oocyte 31
3.1.3 *spir* expression in the nervous system 32
3.1.4 *spir-2* expression in the intestine and testis 33
3.1.5 Summary 34

3.2 Mouse genetic analyses of Spir-1 function **35**
3.2.1 Function of Spir-1 in neuronal differentiation 36
3.2.2 Function of Spir-1 in dendritic spine formation 38

4 MATERIALS AND METHODS 40

4.1 Materials 40
4.1.1 Disposable materials 40
4.1.2 Chemicals and Reagents 42
4.1.3 Cell Culture Media, Reagents and Supplements 44
4.1.4 Antibodies 44
4.1.5 Enzymes 45
4.1.6 Kits 45
4.1.7 Molecular Weight Markers 46
4.1.8 Oligonucleotides 46
4.1.9 Mouse lines 47
4.1.10 Solutions and Buffers 48
4.1.10.1 General buffers 48
4.1.10.2 DNA buffers 50
4.1.10.3 *In situ* hybridization buffers 50
4.1.10.4 Protein buffers 52

4.2 Methods 54
4.2.1 Cell culture methods 54
4.2.1.1 Poly-d-lysine coating 54
4.2.1.2 Isolation of primary mouse cortical neurons 54
4.2.2 Nucleic acid analyses 55
4.2.2.1 DNA Isolation from mouse biopsies 55
4.2.2.2 RNA Isolation from cells and tissues 55
4.2.2.3 RNA concentration measurement 56
4.2.2.4 cDNA-Synthesis 56
4.2.2.5 Polymerase chain reaction (PCR) 56
4.2.2.6 Agarose gel electrophoresis 57
4.2.2.7 Real-time PCR 57
4.2.2.8 Generation of DIG-labeled RNA probes 58
4.2.2.9 *In situ* hybridization 58
4.2.3 Protein analyses 60
4.2.3.1 Preparation of whole protein lysates 60
4.2.3.2 SDS polyacrylamide gel electrophoresis (SDS-PAGE) 60
4.2.3.3 Western Blot 61
4.2.3.4 Immunodetection 61
4.2.4 Immunocytochemistry 62
4.2.5 Histology 62

5 BIBLIOGRAPHY 64

6 APPENDIX 71

6.1 List of abbreviations 71

6.2 Acknowledgements 73

6.3 Curriculum vitae 74

6.4 List of publications 75

1 Introduction

1.1 The actin cytoskeleton

Actin is one of the most highly conserved and abundant proteins in eukaryotic cells. The assembly and disassembly of actin filaments combined with motor proteins of the myosin family are the driving forces of numerous cellular functions, including morphogenesis, migration, cytokinesis and membrane transport (Chhabra and Higgs, 2007; Pollard and Cooper, 2009).

The spatial and temporal initiation of actin polymerization is an essential regulatory element for actin to fulfill its different cellular functions. Actin filaments are built by the assembly of the 42 kDa monomeric globular actin (G-actin) into double stranded helical filaments (F-Actin). Since all actin subunits point in the same direction the filaments are polar, containing a dynamic barbed (+) end (fast-growing end of a filament) and a less active pointed (-) end (slow-growing end of a filament) (Fig. 1.1) (Pollard and Borisy, 2003; Renault *et al*., 2008).

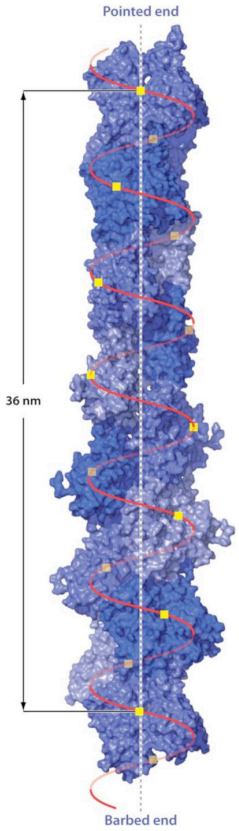

Fig. 1.1 Helical structure of an actin filament (figure from Dominguez and Holmes, 2011)
Details of the actin filament structure have been deduced from cryo-electron microscopy (Fujii *et al*., 2010). The filament is made of two chains that gradually turn around each other. Approximately 13 molecules repeat every six turns in an axial distance of 35.9 nm.

Actin is an ATP binding protein and a critical factor for regulating the transition between G-actin and F-actin is the hydrolysis of ATP (Pollard and Borisy, 2003). Actin hydrolyzes the terminal phosphate from the bound ATP after assembly into filaments and then slowly dissociates the phosphate. This reaction together with subtle changes in the structure of actin subunits arranges ADP-bound actin filaments for the disassembly by regulatory proteins (Pollard and Cooper, 2009).

The polymerization of F-actin from G-actin however, is kinetically unfavorable due to the instability of actin dimers and trimers (Pollard, 2007). Further, in cells a large pool of actin monomers is typically buffered by actin monomer binding proteins, such as thymosin β4 and profilin (Chesarone and Goode, 2009). Therefore the spontaneous actin polymerization is inhibited (Pollard, 2007).

To overcome the kinetic barrier to form a filament from free actin monomers, a process called nucleation, actin nucleation factors are required (Pollard 2007). Actin filaments assemble at least into 15 different structures in metazoan cells and consistent with the diversity of cellular actin structures, different mechanisms exist to nucleate actin filaments (Fig. 1.2) (Chhabra and Higgs, 2007; Pollard, 2007).

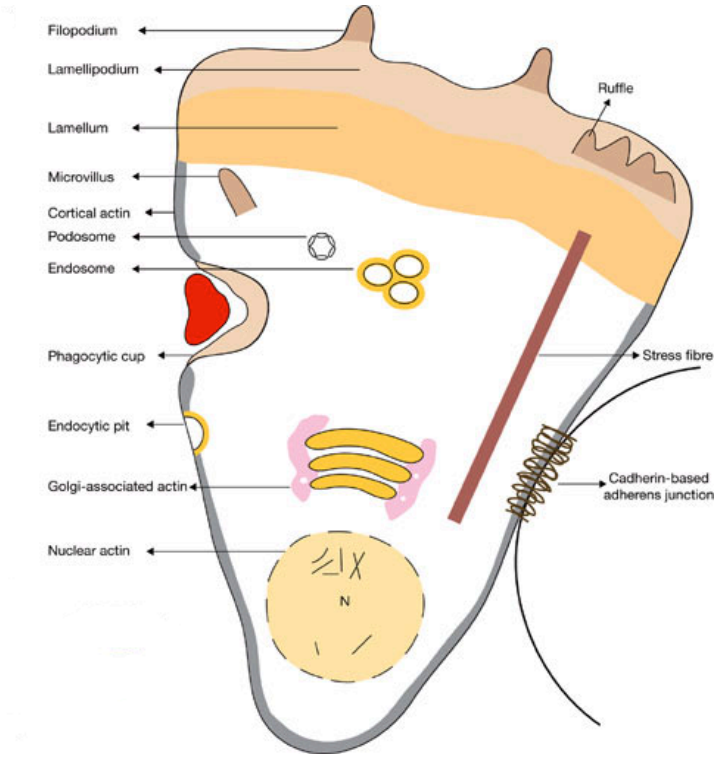

Fig. 1.2 Actin structures in cells (figure adapted from Chhabra and Higgs, 2007)
In metazoan cells actin filaments are assembled into a wide variety of cellular structures. A schematic draw of an upwards-migrating cell, that is attached to another cell on the right, is shown. Actin filaments in different cellular structures are indicated.

1.2 Actin nucleation

To date three major groups of actin nucleation factors have been identified: the Arp2/3 complex and its nucleation promoting factors, FH2 domain containing nucleators of the formin superfamiliy and nucleation factors containing one or multiple Wiskott-Aldrich syndrome protein homology domain 2 (WH2) actin binding domains (Fig.1.3) (Qualmann and Kessels, 2009).

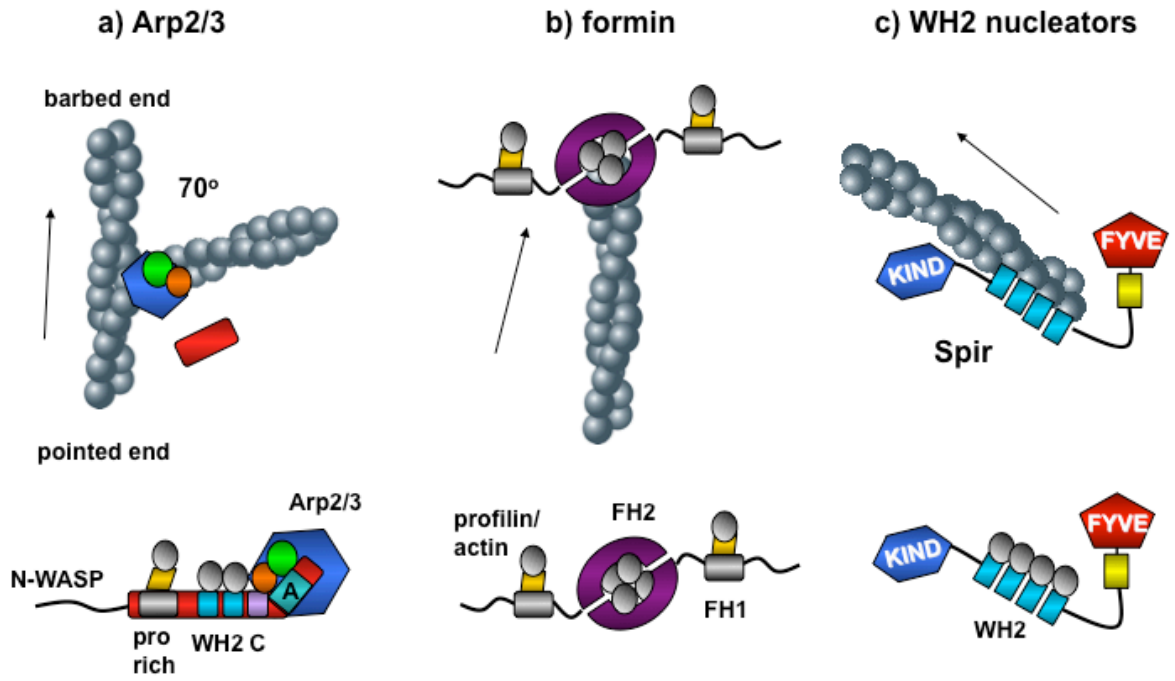

Fig. 1.3 Actin nucleation mechanisms (figure adapted from Kerkhoff, 2006)
a) The Arp2/3 complex consists of seven subunits. It is proposed that the actin-related proteins Arp2 (orange circle) and Arp3 (green circle) mimic a conventional actin dimer, thus overcoming the kinetic barrier to actin nucleation (Aguda *et al*., 2005; Kelly *et al*., 2006). Binding to nucleation promoting factors such as N-WASP activates the Arp2/3 complex, which binds the central (C) sequence and an acidic sequence (A) in the C-terminal part of WASP (Machesky and Insall, 1998). The WH2 domain binds monomeric actin (grey circle) (Paunola *et al*., 2002). A proline rich region attracts profilin-actin (yellow square plus grey circle) to the complex. The Arp2/3 complex binds to sides of preexisting filaments and nucleates new actin filaments at an angle of 70° (Pollard and Beltzner, 2002). **b)** The formin family of actin nucleation factors shares a common formin homology 1 domain (FH1, grey) and a formin homology 2 domain (FH2, purple) in the C-terminal region of the proteins. The FH1 domain is proline rich and binds profilin-actin (yellow square plus grey circle). The FH2 domain crystal structure in complex with tetramethylrhodamine-actin revealed that the FH2 domain forms a ring-like dimer structure, in which two actin proteins are bound to one FH2 domain, in an orientation similar to that in an actin filament (Otomo *et al*., 2005). Upon nucleation formins remain associated as a dimer with the barbed end of the actin filament (Vavylonis *et al*., 2006). **c)** Spir proteins are the founding members of the WH2 domain containing actin nucleation factors. Spir nucleates actin polymerization by binding of actin to a cluster of four WH2 domains in the central part of the protein.

1.2.1 Formins

Formins are large modular proteins that contain a highly conserved formin homology 2 (FH2) domain and an adjacent proline rich formin homology 1 (FH1) domain. (Higgs, 2005). Phylogenetic analyses of the FH2 domains reveal that metazoan formins segregate into eight groups: Dia (diaphanous), DAAM (disheveled-associated activator of morphogenesis), FMNL (formin like protein), FHOD (formin homology domain containing protein), WHIF (WH2 domain containing formin), INF (inverted formin), Delphilin, and Fmn (formin) (Fig. 1.4) (Higgs, 2005; Schönichen and Geyer, 2010).

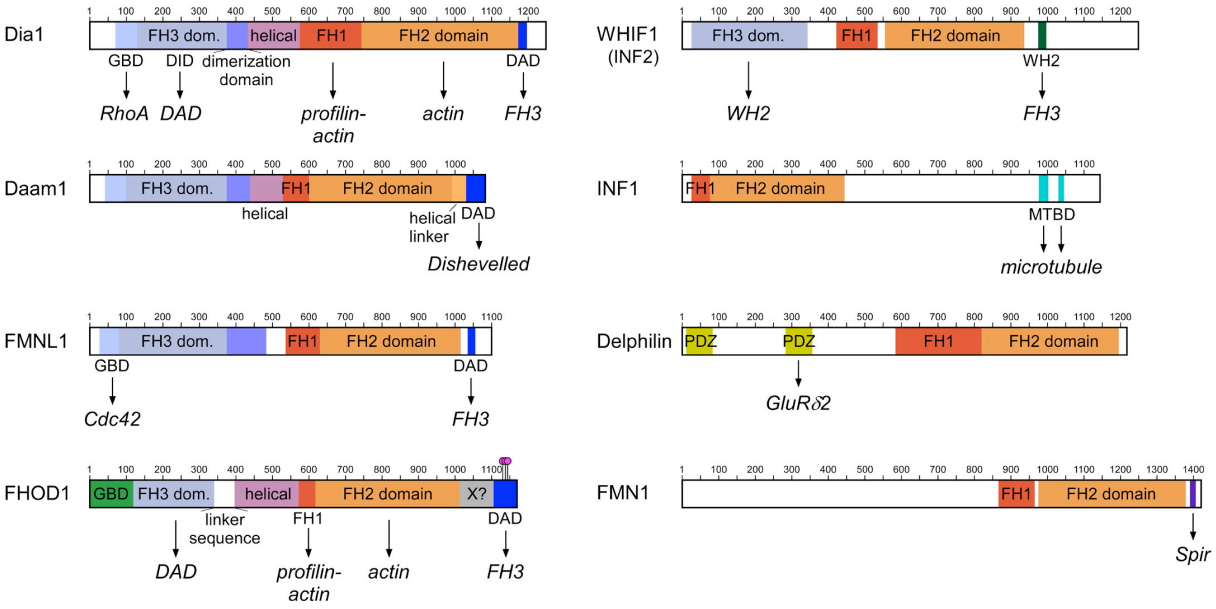

Fig. 1.4 Structural array of human formins (figure from Schönichen and Geyer, 2010)
A schematic draw of the domain architecture of each member from all eight formin families is shown. Following domains are denoted: formin homology 1 domain (FH1), formin homology 2 domain (FH2), formin homology 3 domain (FH3), GTPase binding domain (GBD), the N-terminal Diaphanous inhibitory domain (DID) that is followed by a helical region, the C-terminal Diaphanous autoregulatory domain (DAD). Some formins like WHIF and Delphilin contain a WH2 actin binding domain and PDZ domains, respectively. Arrows below the domains indicate interaction partners as far as known from cellular and biochemical studies.

The FH1 domain, with its high content of proline, is a profilin-actin binding domain (Kovar *et al*., 2003). Profilin accelerates the exchange of ADP to ATP on actin monomers and provides a cellular pool of ATP-actin for new filament assembly (Witke, 2004).

The FH2 domain has been shown to alter actin polymerization dynamics by accelerating *de novo* filament nucleation, altering the rate of filament elongation and

depolymerization and preventing filament barbed end capping by capping proteins (Higgs, 2005). The FH2 domain crystal structure of the yeast formin Bni1p with tetramethylrhodamine-actin has been solved and this structure displays a doughnut-shaped FH2 dimer, in which each of the FH2 domains binds two actin proteins in an orientation corresponding to that in an actin filament (Shimada *et al*., 2004; Xu *et al*., 2004; Otomo *et al*., 2005). After nucleation the FH2 head-to-tail homodimers remain processively associated with the elongating fast growing barbed end of the filament (Romero *et al*., 2004; Kovar, 2006; Vavylonis *et al*., 2006). It is proposed that the FH2 domains are in rapid equilibrium between confirmations that block or enable actin addition and in which the FH1 domain transfers profilin-actin from the multiple profilin binding sites rapidly to the barbed end (Vavylonis *et al*., 2006).

1.2.2 The WH2 domain containing actin nucleation factor Spir

Spir proteins are the founding members of the WH2 domain containing actin nucleation factors (Quinlan *et al*., 2005). They have exclusively been identified in metazoans and share a common structural array. Vertebrate genomes encode two *spir* genes, *spir-1* and *spir-2*, whereby the corresponding proteins, Spir-1 and Spir-2, show a high degree of homology, especially in the evolutionally conserved domain structures (Fig 1.5). All known Spir proteins are composed of an N-terminal kinase non-catalytic C-lobe domain (KIND) and a cluster of four actin binding WH2 domains in the central part of the protein (Ciccarelli *et al*., 2003; Quinlan, 2005). The KIND domain was discovered by sequence alignments with Spir proteins from different species and represents the isolated C-lobe of kinases and is proposed to be catalytically inactive (Ciccarelli *et al*., 2003). It interacts with a highly conserved short sequence motif C-terminal adjacent to the FH2 domain of formin (formin Spir interaction sequence, FSI) (Pechlivanis *et al*., 2009; Zeth *et al*., 2011).

The C-terminal part of Spir encodes a potential Rab GTPase binding site, the Spir-box, and a modified FYVE zinc-finger membrane localization domain (Fig. 1.5) (Otto *et al*., 2000). The Spir-box is a highly conserved region and shares sequence homology with an α-helical region of rabphilin-3A, which mediates the interaction between rabphilin-3A and the GTP-loaded small G protein Rab3A (Ostermeier and Brunger, 1999; Kerkhoff *et al*., 2001). The modified FYVE zinc finger domain is located C-terminal adjacent to the Spir-box. FYVE domains contain eight cysteine residues that bind two zinc ions and form a hydrophobic “turret loop”, which penetrates the membrane (Misra and Hurley, 1999; Hurley, 2006). The FYVE domain of Spir however is different; it lacks a basic pocket that specifically binds to phospholipid phosphatidylinositol 3-phosphate (PI(3)P), suggesting that Spir has

different phospholipid binding properties compared to other FYVE domain containing proteins.

The nucleation activity of Spir resides in the cluster of the four WH2 domains (WH2 A-D), which are separated by three conserved linker regions (L 1-3). It is proposed that two actin monomers bind to the C-terminal WH2 domains WH2-D and WH2-C, thereby forming an initial actin dimer. Thus, linker 3 overcomes the kinetic barrier of dimer formation by coordinating actin monomers in a structure that is believed to lie along one strand of the longpitch actin helix. Actin monomers from WH2-B and WH2-A are further stacked onto this prenucleus and a longitudinal tetramer is formed. After formation of the complete nucleus, rapid polymerization proceeds. (Quinlan *et al*., 2005; Kerkhoff, 2006).

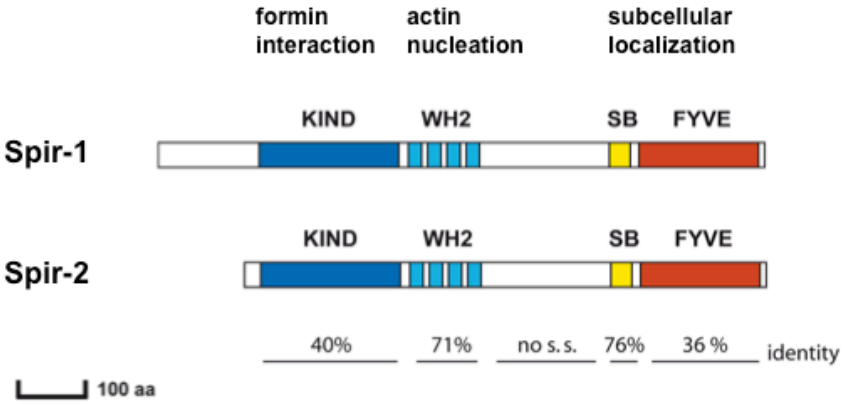

Fig. 1.5 Structure of mammalian Spir proteins (figure from Pleiser *et al*., 2010)
Spir proteins encode a KIND protein interaction module at their N-terminal end. Four WH2 domains are located in the central part of the protein and are sufficient for actin nucleation. The Spir-box (SB) and the FYVE zinc finger, which are located at the C-terminal part of Spir mediate the subcellular localization. The structure of the mammalian Spir-1 and Spir-2 proteins is shown with a scale bar representing 100 amino acids (aa). The results of sequence alignments of the underlined regions of Spir-1 versus Spir-2 are given in percent identity. The identity scores have been determined with the NCBI Blast alignment tool. For several regions no significant similarity (no s.s) could be detected.

1.2.3 Spir/formin cooperation in actin nucleation

Although Spir proteins can nucleate actin polymerization *in vitro* by themselves, genetic, cell biological and biochemical studies demonstrate that Spir cooperates with the distinct actin nucleators of the formin subgroup of formins (*Drosophila melanogaster* Cappuccino protein and its two vertebrate homologues formin-1 and formin-2 (Quinlan *et al*., 2007; Pechlivanis *et al*., 2009; Pfender *et al*., 2011).

Drosophila mutants of *spire* and *cappuccino* were found in the same genetic screen, which revealed that both mutants have an identical phenotype (Manseau and Schupbach, 1989; Wellington *et al*., 1999). Both nucleators cooperate in the generation of a dynamic actin mesh in the *Drosophila* oocyte, which suppresses premature ooplasmic streaming (Dahlgaard *et al*., 2007).
Spir and formin subgroup family proteins physically interact with each other. It was shown that the N-terminal Spir KIND domain interacts with the C-terminal part of the formin protein comprising the FH2 domain and flanking regions (Quinlan *et al*., 2007) and *in vitro* actin polymerization assays revealed that the interaction enhances the nucleation activity of Spir and blocks the formin activity (Quinlan *et al*., 2007)

Evidence has been raised that this regulatory interaction is evolutionally conserved among flies and mammals. Both *Drosophila* proteins, Spir and Cappuccino have two mammalian homologues, Spir-1 and Spir-2 and formin-1 (Fmn-1) and formin-2 (Fmn-2). The mouse genes have a very restricted and nearly identical expression pattern. During mouse embryogenesis *spir-1* and *formin-2* expression exactly overlaps in the nervous system. In the adult brain high expression of both gens was found in the Purkinje cells of the cerebellum and in neuronal cells of the hippocampus and dentate gyrus (Schumacher *et al*., 2004).
Very recently mouse Spir-1 and Spir-2 were described to cooperate with the mouse Cappuccino homolog formin-2 protein in regulating an actin meshwork in mouse oocytes that is required for asymmetric spindle positioning during meiosis. Additionally, the proteins colocalized at the cleavage furrow during polar body extrusion, which was found to be dependent on Spir function (Pfender *et al*., 2011). The collaboration between Spir and formin is therefore considered to be a major regulatory function in mammalian oocyte maturation and is thought to be an essential mechanism in reproduction. Consistently, hypofertility was identified as a major phenotype of formin-2 deficient mice (Leader *et al*., 2002).

In line with these genetic and cellular studies, biochemical analyses revealed that mouse Spir and formin proteins show the same regulatory interaction as their *Drosophila* homologues (Quinlan *et al*., 2007; Pechlivanis *et al*., 2009; Zeth *et al*., 2011). It was shown that both mammalian formin subgroup proteins, formin-1 and formin-2 interact with both mammalian Spir proteins, Spir-1 and Spir-2. It could however be demonstrated that not the FH2 domain mediates the interaction with the KIND domain of Spir, but a highly conserved short sequence motif C-terminal adjacent to the FH2 domain (formin Spir interaction sequence, FSI) (Pechlivanis *et al*., 2009). The crystal structure of the Spir-1-KIND/Fmn-2-FSI complex has recently been solved, showing that basic formin sequences contact an acidic groove on the Spir KIND surface (Vizcarra *et al*., 2011; Zeth *et al*., 2011).

Fig. 1.6 displays the current model of Spir and formin cooperation in actin nucleation and polymerization. Both proteins bind with a ratio of one Spir molecule per formin FH2 subunit. With their C-terminal FYVE-like zinc finger motifs, Spir proteins might dimerize by binding to intracellular membranes. This stoichiometry brings eight WH2 domains in proximity to each other, which explains the increasing nucleation activity of Spir. It is proposed that the Spir-nucleated filament is arranged with its barbed end facing formin. The proline rich FH1 domain of formin is a profilin-actin binding domain. Profilin is an actin monomer binding protein that accelerates the ADP-ATP exchange on actin monomers, thus providing a cellular pool of ATP-actin for new filament assembly. Possibly the FH1 domain compensates for the lack of profilin binding by Spir. It is speculated that after the KIND-FH2 interaction is released, the formin protein subsequently polymerizes the initiated actin filament (Quinlan and Kerkhoff, 2008).

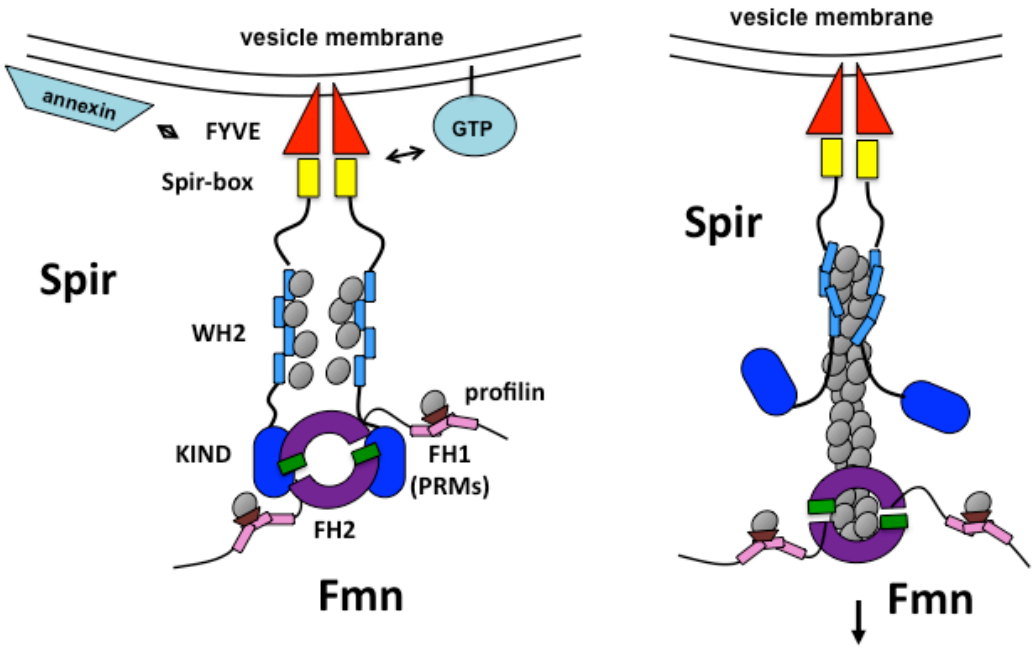

Fig. 1.6 Model of Spir/formin cooperation in actin nucleation (figure adapted from Kerkhoff, 2011)

A model is proposed in which Spir is targeted towards intracellular membranes via its FYVE zinc finger motif. This localization might be induced by a possible dimerization of Spir proteins and a potential interaction with annexin A2 or a GTP binding protein of the Ras superfamily. Spir proteins form a regulatory complex with the distinct actin nucleator of the formin subgroup of formins (Fmn). It is proposed that Spir attracts formin to the membrane via the Spir-KIND/Fmn-FSI interaction. Upon the nucleation of an actin filament by binding of actin monomers to the Spir WH2 domains, the Spir/formin interaction is released and formin polymerizes the initiated actin nucleus. Thereby formin remains associated with the elongating barbed end. It has been suggested that actin bound to the FH1 domain through profilin can be rapidly transferred to the barbed end of the growing filament. Following structures are highlighted: FYVE (red), Spir-box (SB) (yellow), WH2 (light blue), KIND (dark blue), FH1 (rose), FH2 (purple), FSI (green), actin (grey), profilin (brown). Abbreviations: PRMs: proline rich motif.

1.3 Spir function in vesicle transport processes

From the beginning of the discovery of the Spir protein, its domain structure proposed a function of Spir in actin organization at intracellular membranes (Otto *et al*., 2000; Kerkhoff *et al*., 2001). The FYVE zinc finger domain, which is located in the C-terminal part of the Spir protein, is a domain typically found in proteins involved in membrane trafficking (Misra and Hurley, 1999) (Stenmark *et al*., 1996). Spir proteins localize at distinct cytoplasmic spots when transiently expressed in mammalian cells, where they induce actin filament formation (Kerkhoff, 2011). This specific localization depends on the integrity of the FYVE zinc finger domain and the Spir-box, which is N-terminal adjacent to the FYVE domain and is a potential Rab small G protein interaction module (Kerkhoff *et al*., 2001). Mutation of the FYVE zinc finger or deletion of the Spir-box causes an even cytoplasmic distribution of the mutant proteins (Kerkhoff *et al*., 2001). When transiently expressed, Spir proteins largely colocalize with the small G-protein Rab11, which is located at the trans-Golgi network, post-Golgi vesicles and the recycling endosome (Sönnichsen *et al*., 2000; Kerkhoff *et al*., 2001). Spir proteins are involved in exocytic transport processes and the transport beyond early endosomes (Morel *et al*., 2009; Kerkhoff *et al*., 2001). Overexpression of a truncated Spir protein, that lacks the KIND domain and WH2 domains (Spir-1-CT), inhibits the transport of the vesicular stomatitis virus G protein (VSV G) to the plasma membrane, suggesting a role for Spir in the secretory pathway (Kerkhoff *et al*., 2001). In addition, the formation of actin patches on enlarged early endosomes was inhibited as well as the transport of dextran to late endosomes after knocking-down the *spir-1* gene via siRNA (Morel *et al*., 2009).

1.4 Aim of the work

Extensive biochemical and structural studies have been performed to understand the Spir actin nucleation mechanism and its cooperation with formin proteins. Only little is known today about the cell biological function of Spir proteins. From the beginning of the Spir protein discovery, its structural domain characterization proposed a function of Spir in actin organization at intracellular membranes. In mammalian cells, Spir is targeted towards intracellular membranes via the C-terminal modified FYVE zinc finger motif and the N-terminal adjacent Spir-box, which is a potential Rab GTPase interaction site. Spir proteins have been implicated in exocytic transport processes and the transport beyond early endosomes. The function of Spir/formin nucleated actin polymerization at intracellular membranes as well as the signaling cascades regulating the activity of the Spir/formin complex however, are still unknown.
Earlier studies of the mouse *spir-1* gene revealed a very restricted expression, which mainly resides in neuronal cells of the nervous system. Within the scope of this work the yet unknown expression pattern of the mouse *spir-2* gene was analyzed in order to gain more insights into Spir function during mouse development and in adult mouse tissues. To further reveal cell biological functions of Spir, a mouse genetic approach was chosen to specifically impair the function of the Spir-1 protein.

2 Results

2.1 Tissue specific expression of the mouse *spir-1* and *spir-2* genes

2.1.1 Relative mRNA expression of *spir-1* and *spir-2*

Spir expression is restricted to metazoans of the animal kingdom. No *spir* genes were identified in plants and single cell organisms such as yeast. The vertebrate genomes encode two *spir* genes, *spir-1* and *spir-2* (Kerkhoff, 2006).

Real-time polymerase chain reaction (PCR) allows the relative quantification of gene expression in relation to a housekeeping gene and can therefore be used to compare expression levels of different genes. In order to get an initial overview of *spir-2* expression in adult mouse tissues and to quantify and compare the gene expression levels of the two mouse *spir* genes, real-time PCR was performed. cDNA templates from different tissues have been generated by reverse transcription of total mRNA preparations.

The by far highest expression of both, *spir-1* and *spir-2* was detected in mouse oocytes. Additionally, both genes are highly expressed in testis and brain (telencephalon and cerebellum). However, *spir-2* shows a much broader expression pattern than *spir-1*; it is further expressed throughout the digestive tract (stomach, small intestine, large intestine) and kidney. Only a weak expression of *spir-1* is found in spleen, kidney and stomach (Fig. 2.1).

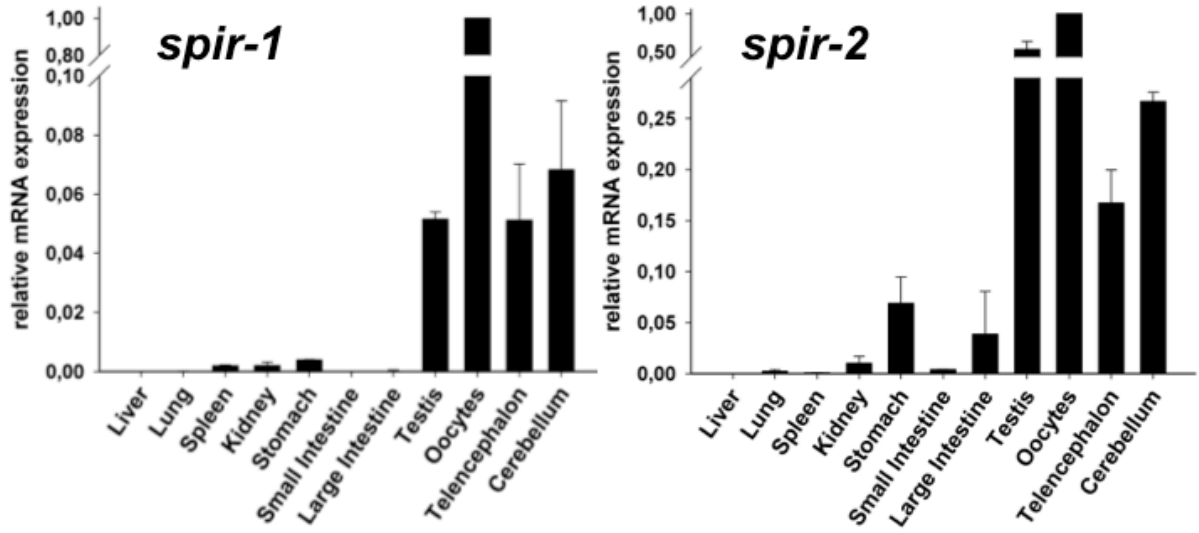

Fig. 2.1 Relative gene expression analysis of *spir-1* and *spir-2*

The relative expression of *spir* genes has been analyzed by real-time PCR. Total RNA of the indicated mouse tissues has been prepared. cDNA has been generated by reverse transcription and used as template. Specific DNA primers were employed to amplify the *spir-1* and *spir-2* genes and as a standard housekeeping gene, the *β-microglobulin* gene. The relative amount of target mRNA normalized to *β-microglobulin* was calculated and is shown in a bar diagram for each gene. mRNA levels were then compared to those in oocytes. Data are means ± s.d from two different experiments.

2.1.2 *spir-2* gene expression during mouse embryogenesis

To determine the spatial and temporal expression of the *spir-2* gene during mouse embryogenesis, *in situ* hybridization analyses on whole embryo sagittal sections from embryonic stages E11.5, E13.5, E15.5, and E17.5 were performed. Already at embryonic day 11.5 (E11.5) expression of *spir-2* is evident throughout the central nervous system, including forebrain, midbrain, hindbrain and spinal cord. The intense expression in the CNS, especially in the forebrain, remains strong until late stages of embryonic development (E17.5). *spir-2* expression seems to increase in the cerebral cortex during its development. In the peripheral nervous system *spir-2* is clearly detected in the dorsal root ganglia from embryonic stages E11.5 - E15.5. At E13.5 and E15.5 transcripts for *spir-2* are also observed in the trigeminal ganglion (Fig. 2.2a) (Pleiser *et al*., 2010).

In situ hybridizations on coronal brain sections from embryonic stages E11.5, E14.5 and E17.5 confirmed the high *spir-2* expression in the central nervous system throughout development. At E11.5 *spir-2* expression is apparent in the ventricular zone of the lateral and third ventricle as well as the cerebral aqueduct and along the wall of the fourth ventricle (Fig. 2.2b, left panels). At later stages of development *spir-2* transcripts are consistently found in fore-and midbrain with strongest expression in the ventricular zone (vz), the lateral ganglionic eminence (lge), the neopallial cortex (cx) and thalamus (th) (Fig 2.2b, middle and right panels). No *spir-2* expression is found in the hippocampus at embryonic day 17.5 (Fig. 2.2b, lower right panel) (Pleiser *et al*., 2010).

In situ hybridizations on adjacent cross sections through the mid-thoracic region of the embryo at different mid-gestational stages were performed in order to analyze *spir* expression in the neural tube. The corresponding level of spinal cord for embryonic stage E11.5 and E15.5 is indicated in Fig. 2.2a (dashed line). A cross section of the developing neural tube at embryonic day 11.5 reveals *spir-2* expression in the mantle layer, the ventral horn and in dorsal root ganglia (Fig. 2.2c, upper left panel) whereas strongest *spir-1* expression is seen in the ventricular zone and the dorsal horn of the neural tube (Fig. 2.2c, lower left panel) (Pleiser *et al*., 2010). At embryonic day 14.5 both *spir* genes are expressed in the dorsal and ventral horns of the neural tube, areas that will eventually form the grey matter, as well as in dorsal root ganglia (Fig. 2.2c, middle panels). *spir-1* expression is enriched in the ventricular zone at that stage of development, whereas *spir-2* shows an even expression throughout the neural tube. At E15.5 both, *spir-2* and *spir-1* are evenly expressed within the neural tube and display an identical expression pattern (Fig. 2.2c, right panels) (Pleiser *et al*., 2010).

In the developing eye at embryonic day 17.5 *spir-2* is strongly expressed in the postmitotic retina (Fig 2.2d, left panel). The same expression was already observed at embryonic day 15.5 (Fig 2.2a, eye, e) (Pleiser *et al*., 2010).

The real-time PCR analysis revealed high expression of *spir-2* throughout the intestinal tract in adult mouse tissues (Fig. 2.1, right panel). *In situ* hybridization revealed first expression of the *spir-2* gene at embryonic day 17.5 in the developing intestine (Fig. 2.2d, right panel). There was no staining in intestine for *spir-2* at embryonic day 15.5 (Fig. 2.2a, intestine, i) (Pleiser *et al*., 2010).

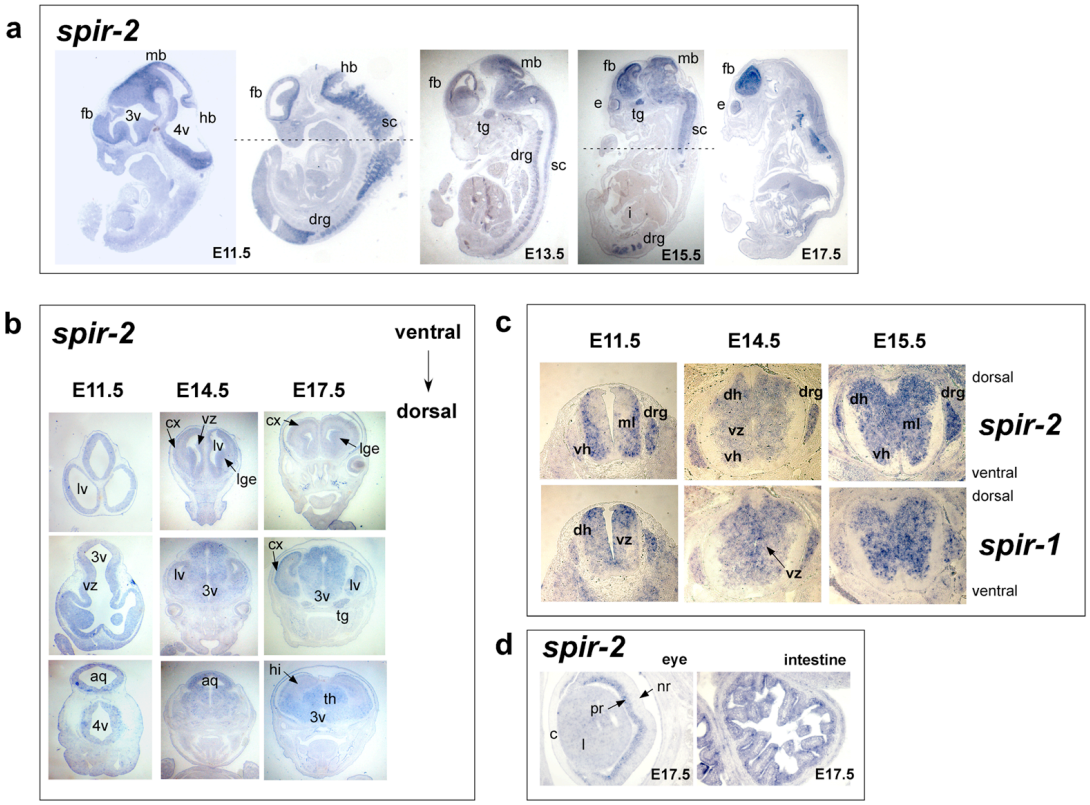

Fig. 2.2 Expression of the mouse *spir-2* gene during mouse embryogenesis

a) Expression of the *spir-2* gene of embryonic day 11.5 (E11.5), 13.5 (E13.5), 15.5 (E15.5), and 17.5 (E17.5) mouse embryos. *In situ* hybridizations on sagittal sections of whole mouse embryos of the indicated embryonic developmental stages were performed. Regions of *spir-2* expression have been marked: fb, forebrain; mb, midbrain; hb, hindbrain; 3v, third ventricle; 4v, fourth ventricle; tg, trigeminal ganglion; sc, spinal cord; drg, dorsal root ganglia; e, eye. At E15.5 *spir-2* is not yet expressed in the intestine, i. Dashed lines indicate level of spinal cord corresponding to the cross section shown in Fig. 2.2c for embryonic stages E11.5 and E15.5. **b)** *In situ* hybridizations on coronal brain sections of day 11.5 (E11.5), 14.5 (E14.5) and 17.5 (E17.5) mouse embryos show *spir-2* transcripts evenly distributed throughout the brain. Marked regions: lv, lateral ventricle; 3v, third ventricle; 4v, fourth ventricle; aq, cerebral aqueduct; cx, neopallial cortex; vz, ventricular zone; lge, lateral ganglionic eminence; tg, trigeminal ganglion; hi, hippocampus; th, thalamus. **c)** Expression of the *spir-2* and *spir-1* genes in the neural tube of day 11.5 (E11.5), 14.5 (E14.5) and 15.5 (E15.5) mouse embryos. *In situ* hybridizations of cross sections of the indicated *spir-2* and *spir-1* genes are shown. Regions of expression are marked: vz, ventricular zone; ml, mantle layer; vh, ventral horn; drg, dorsal root ganglia. **d)** Expression of the *spir-2* gene in the developing eye and intestine. *In situ* hybridizations on a sagittal section of the eye and the intestine of an embryonic day 17.5 (E17.5) mouse embryo are shown. The following regions are marked: c, cornea; l, lens; pr, postmitotic retina; nr, neuroblastic retina.

From Pleiser *et al*., 2010

2.1.3 Spatial *spir-2* gene expression in adult mouse tissues

The initial real-time PCR experiments showed high expression of the mouse *spir-2* gene in oocytes, testis, brain, the digestive tract and kidney. In order to define the cellular nature of *spir-2* expression in these tissues, *in situ* hybridizations were performed. In a horizontal section of the adult brain, *spir-2* mRNA expression was detected in the external capsule (ec), the thalamus (th), the external and central nucleus of the inferior colliculus as well as the intercollicular nucleus (ecic, cnic) and the cerebral cortex (cx) (Fig. 2.3a, left panel). Very high expression is observed in the cerebellum (Fig. 2.3a, cb). Strong staining is seen in the Purkinje cell layer (pcl) and the granular cell layer (gcl) (Fig. 2.3b) (Pleiser *et al*., 2010).

In situ hybridization on a horizontal adult mouse brain section, using a *spir-1* specific riboprobe, reveals *spir-1* expression in the Purkinje cells of the cerebellum (cb) as well as in the CA1, CA2 and CA3 regions of the hippocampus (hi) and the dentate gyrus (Fig. 2.3a, right panel). Additional *spir-1* expression can be observed in the thalamus (th), the anterodorsal nucleus (ad), the lateral septal nucleus and septohippocampal nucleus (lsd), was well as the cortex (cx) (Fig. 2.3a, right panel). *spir-1* expression is substantially increasing from the temporal to the frontal cortex, with strongest expression in the prelimbic cortex, infralimbic cortex and ventral-, medial- and lateral-orbital cortex (Pleiser *et al*., 2010).

By real-time PCR analysis four other tissues were found to have high expression of the *spir-2* gene: the digestive tract, testis, kidney and oocytes. The expression of *spir-2* in these tissues has as well been analyzed. Fig. 2.3c displays *in situ* hybridizations on an oblique cross section (upper left panel) and a cross section (lower left panel) of the small intestine. The data reveal *spir-2* mRNA expression in intestinal epithelial cells along villi and crypts. The epithelial expression of *spir-2* was also found in colon (data not shown). To analyze the cellular localization of *spir-2* transcripts in testis, *in situ* hybridization was performed on cross sections of the adult mouse testis. Seminiferous tubules were specifically stained (Fig. 2.3c, upper right panel) with strong expression in spermatocytes (Fig. 2.3c, lower right panel). No expression could be detected in spermatogonia (Fig. 2.3c, spg) (Pleiser *et al*., 2010).
To substantiate the localization of *spir-2* expression in kidney *in situ* hybridizations were performed as well, however, in these experiments no specific cellular expression could be detected (data not shown).

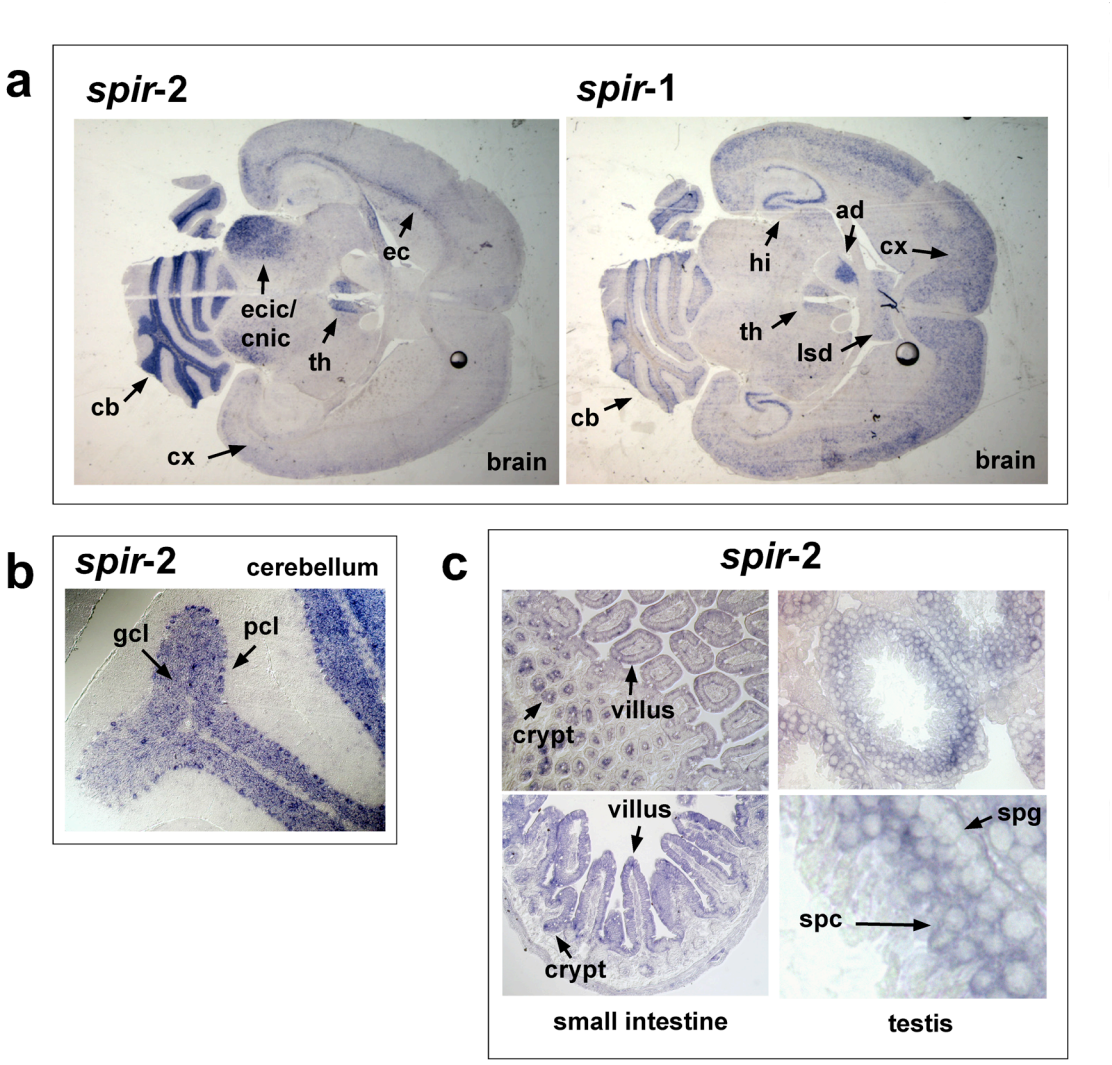

Fig. 2.3 Expression of the mouse *spir-2* gene in adult mouse tissues

a) Horizontal sections of the complete adult mouse brain have been analyzed for *spir-2* and *spir-1* expression. Regions of *spir-2* and *spir-1* expression, respectively, have been marked by arrows: ec, external capsule; th, thalamus; ecic, cnic, external and central nucleus of inferior colliculus, intercollicular nucleus; cb, cerebellum; cx, cerebral cortex; hi, hippocampus; ad, anterodorsal nucleus; lsd, lateral septal nucleus. **b)** A horizontal section of the cerebellum shows expression of the *spir-2* gene in the Purkinje cell layer (pcl) and in the granular cell layer (gcl). **c)** Cross sections of the small intestine (left panels; upper panel is an oblique cross section) and testis (right panels) have been analyzed by *in situ* hybridization for *spir-2* expression. Two different magnifications are shown of each tissue. Marked regions: crypt; villus; spg, spermatogonia; spc, spermatocytes.
From Pleiser *et al*., 2010

2.2 Mouse genetic analyses

2.2.1 Generation of Spir-1 deficient mice

A gene trap approach has been used to generate Spir-1 deficient mice. The *spir-1*$^{gt/+}$ transgenic mice were generated by the Texas A&M Institute for Genomic Medicine (TIGM). Murine embryonic stem (ES) cells from the TIGM 129SvEv gene trap library (clone OST416113), with a gene trap inserted into the fifth predicted intron of the mouse *spir-1* gene were employed. The gene trap disrupts the *spir-1* mRNA at sequences encoding a region immediately downstream of the N-terminal Spir-1 KIND domain (Fig. 2.4a). The gene trap cassette is inserted into a retroviral vector and contains a splice acceptor site (SA) site followed by a promoterless selectable marker neomycin (NEO), with a polyadenylation signal (Fig. 2.4a). The gene trap cassette is transcribed from the endogenous *spir-1* promoter and a fusion transcript is generated in which the predicted *spir-1* exons upstream of the insertion (exons E1-E5) are fused in frame to the *neomycin* marker gene (Fig. 2.4a). In addition the trapping vector contains a mouse *phosphoglycerate kinase* (*PGK*) promoter sequence, followed by a first exon from *bruton's tyrosine kinase* (*BTK*), and a splice donor (SD) site. *spir-1* exons downstream of the gene trap insertion site are spliced to the *bruton's tyrosine kinase* exon, giving rise to another fusion transcript. The *BTK* exon contains stop codons in all three reading frames to prevent translation of the downstream fusion transcript (Fig. 2.4a).

Targeted 129SvEvBrd ES cells were selected for blastocyst microinjection into C57BL/6 mice to produce chimeric mice (TIGM mouse accession: NM_194355.2). Two heterozygous *spir-1*$^{gt/+}$ males and two heterozygous *spir-1*$^{gt/+}$ females were handed out by TIGM and were further bred and analyzed in our laboratory. The provided mice were intercrossed and pubs were monitored daily until weaning.
All mice were kept under standard conventional conditions in the animal facility of the University Hospital of Regensburg. Food and tap water were provided *ad libitum*. Offspring were weaned at 21-30 days of age. After weaning males were housed separately from females. Each mouse was marked by ear clip and a tail biopsy was taken to identify the genotype of each animal. All mice analyzed were of mixed genetic background (129/SvEvBrd and C57BL/6).

The knock-out of *spir-1* expression was confirmed by RT-PCR analysis of brain RNA preparations from wildtype and homozygous *spir-1*$^{gt/gt}$ mice (Fig. 2.4b). Consistent with the gene trapping strategy, a primer set amplifying sequences encoding the N-terminal Spir-1 KIND domain upstream of the gene trap integration (primer set 1), amplified a DNA fragment from wildtype and *spir-1*$^{gt/gt}$ brain RNA preparations,

whereas a primer set with one primer upstream and one primer downstream of the integration site (primer set 2) amplified a DNA fragment from brain RNA of wildtype mice but not from RNA preparations of homozygous *spir-1*$^{gt/gt}$ mice. The corresponding absence of Spir-1 protein expression in homozygous *spir-1*$^{gt/gt}$ mice was confirmed by immunoblot. We have identified the endogenous Spir-1 protein with the help of a rabbit polyclonal antibody raised against a C-terminal Spir-1 peptide (AGPSEYCPSERTINEI) before (Schumacher *et al*., 2004). The endogenous Spir-1 protein migrates with an apparent molecular weight of 95 kDa on a SDS polyacrylamide gel. Total protein lysates of cultured primary cortical neurons isolated from wildtype (wt) and homozygous *spir-1*$^{gt/gt}$ mice were analyzed by immunoblot employing the rabbit polyclonal anti-Spir-1 antibody. The lysate of neuronal cells from the homozygous *spir-1*$^{gt/gt}$ mice showed a specific loss of the 95 kDa band of the endogenous Spir-1 protein, documenting the Spir-1 deficiency of the mice (Fig. 2.4c).

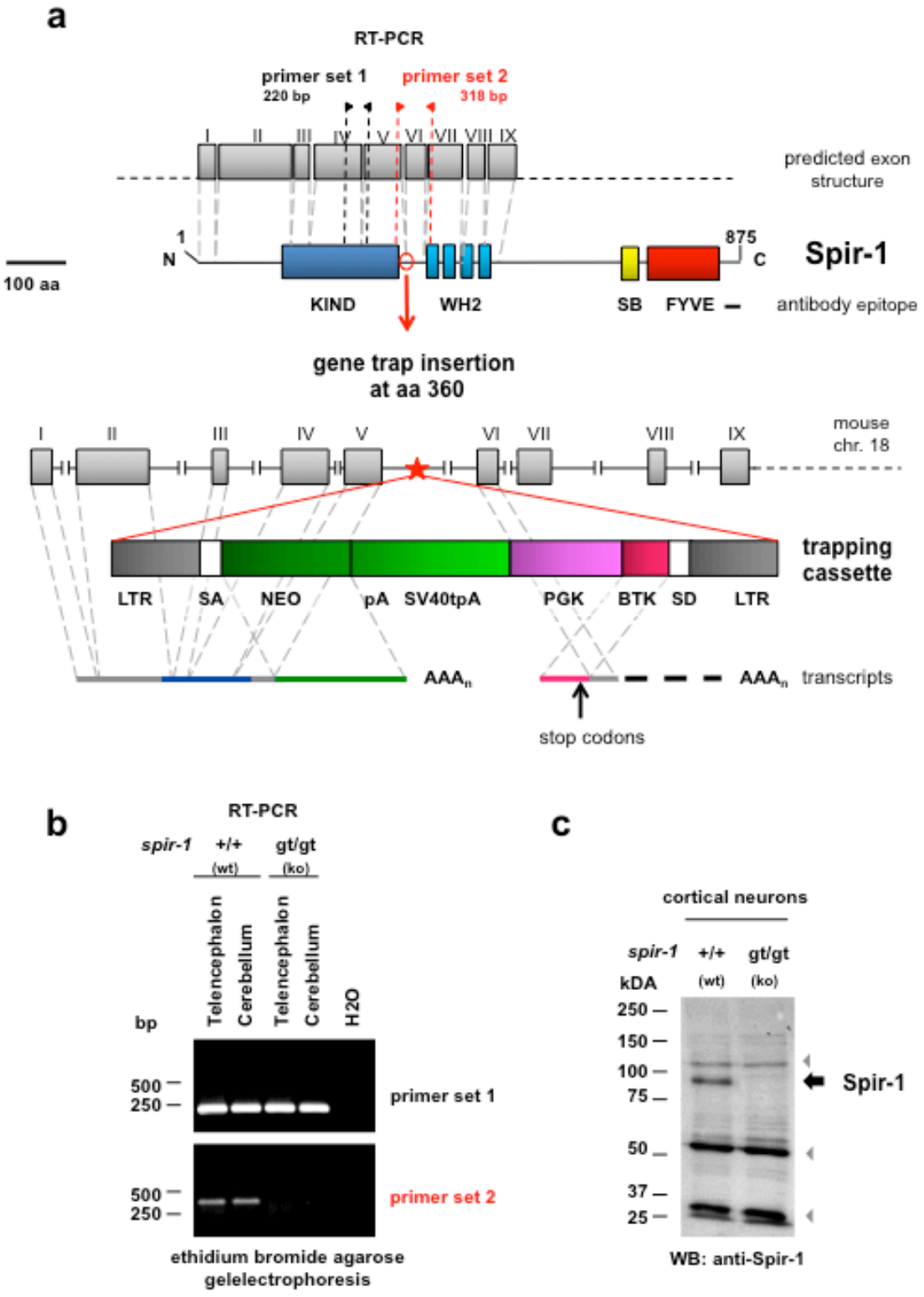

Fig. 2.4 Generation of Spir-1 deficient mice

a) Spir-1 deficient mice were generated by a gene trap insertion into intron V of the predicted mouse *spir-1* gene locus on chromosome 18. The insertion abrogates *spir-1* expression at amino acid 360, immediately downstream of the N-terminal Spir-1 KIND domain. The structure of the Spir-1 protein, the partial predicted exon structure and the gene trap vector are shown. **b)** The insertion of the gene trap vector was confirmed by reverse transcription PCR analysis (RT-PCR). Total RNA of mouse

telencephalon and cerebellum from *spir-1*$^{+/+}$ and *spir-1*$^{gt/gt}$ mice, respectively has been isolated and cDNA has been generated. A DNA primer pair amplifying KIND domain sequences upstream the gene trap insertion site (primer set 1) and a primer pair with one primer encoding sequences of the KIND domain upstream the gene trap insertion and one primer encoding sequences of the WH2 cluster downstream the gene trap insertion site (primer set 2) were employed **c)** The absence of Spir-1 protein expression in *spir-1*$^{gt/gt}$ mice was confirmed by Western blot. Total protein lysates from wildtype and Spir-1 deficient cortical neurons were electrophoresed by SDS polyacrylamide gel electrophoresis, subsequently immunoblotted and analyzed using a Spir-1 antibody. The endogenous Spir-1 protein migrates with a molecular weight of 95 kDa on a SDS polyacrylamide gel (black arrow). Grey arrowheads indicate non-specific protein bands. Abbreviations: aa: amino acids, bp: basepairs, BTK: first exon of the murine Bruton's tyrosine kinase gene, chr: chromosome, LTR: long terminal repeat, NEO: neomycin phosphotransferase gene, pA: polyadenylation sequence, PGK: phosphoglyceratekinase-1 promoter, SA: splice acceptor sequence, SD: splice donor sequence, WB: Western Blot.

2.2.2 Initial phenotyping of Spir-1 deficient mice

Heterozygous male and female *spir-1*$^{gt/+}$ mice were intercrossed and after weaning at postnatal day 21-30, tail biopsies were taken from each mouse and the genotype was determined by PCR analysis.

Homozygous *spir1*$^{gt/gt}$ male and female mice are viable and a macroscopic examination revealed no apparent abnormalities of the skin, skeleton or vital organs. To assess microscopic defects, H&E paraffin sections of every organ from Spir-1 deficient mice and wildtype littermates were prepared and analyzed with assistance of PD Dr. Frauke Bataille and Dr. med. Katharina Schardt from the Pathology department of the University Hospital Regensburg. Also here, no obvious histological defects were found (data not shown). Thus, male and female *spir-1*$^{gt/gt}$ mice were phenotypically normal. Genotyping of the progeny from cross-matings of heterozygous *spir-1*$^{gt/+}$ mice revealed that they were born at normal Mendelian ratios (Tab. 2.1).

Since the real-time PCR analyses revealed highest expression of both *spir* gens in testis and oocytes, the fertility of Spir-1 deficient mice was of special interest. However, no reduced fertility of Spir-1 deficient male and female mice was observed.

Age		No. of mice with genotype			Total No.
	spir-1	+/+	+/gt	gt/gt	
P30		31	52	24	107
	(f/m)	(15/16)	(26/26)	(13/11)	(54/53)

wt	het	ko
29%	49%	22%

Tab. 2.1 Genotypes of progeny from cross-matings of heterozygous *spir-1*$^{gt/+}$ mice

Abbreviations: P30, postnatal day 30; f, female; m, male; wt,wildtype; het, heterozygous; ko, knock-out

2.2.3 Spir-1 function in neuronal differentiation

2.2.3.1 Reduced number of dendritic branchpoints in Spir-1 deficient cultured primary cortical neurons

The Spir-1 deficient homozygous *spir-1*$^{gt/gt}$ mice are a perfect source to study the function of Spir-1 in cell culture experiments with primary cells. To investigate whether the lack of Spir-1 would lead to impaired neuronal differentiation, primary cortical neurons from wildtype and *spir-1*$^{gt/gt}$ E14.5 old embryos were cultured. After four days in culture, the morphology of wildtype and Spir-1 deficient neurons was compared. Dendrites were visualized by immunofluorescence using a MAP2 antibody that specifically stains neuronal dendrites. Primary dendrites emerging from the soma from 25 neurons per genotype were counted. Also the dendritic length was determined by tracing all dendritic processes with the software from *Leica* (*Leica Application Suite Advanced Fluorescence*) and the number of dendritic branchpoints was quantified.

These studies revealed a reduction of neurite branching in cells from Spir-1 deficient embryos. Neither the average length of the dendrites nor the average number of neurites per cell was affected by the lack of Spir-1 (Fig. 2.5).

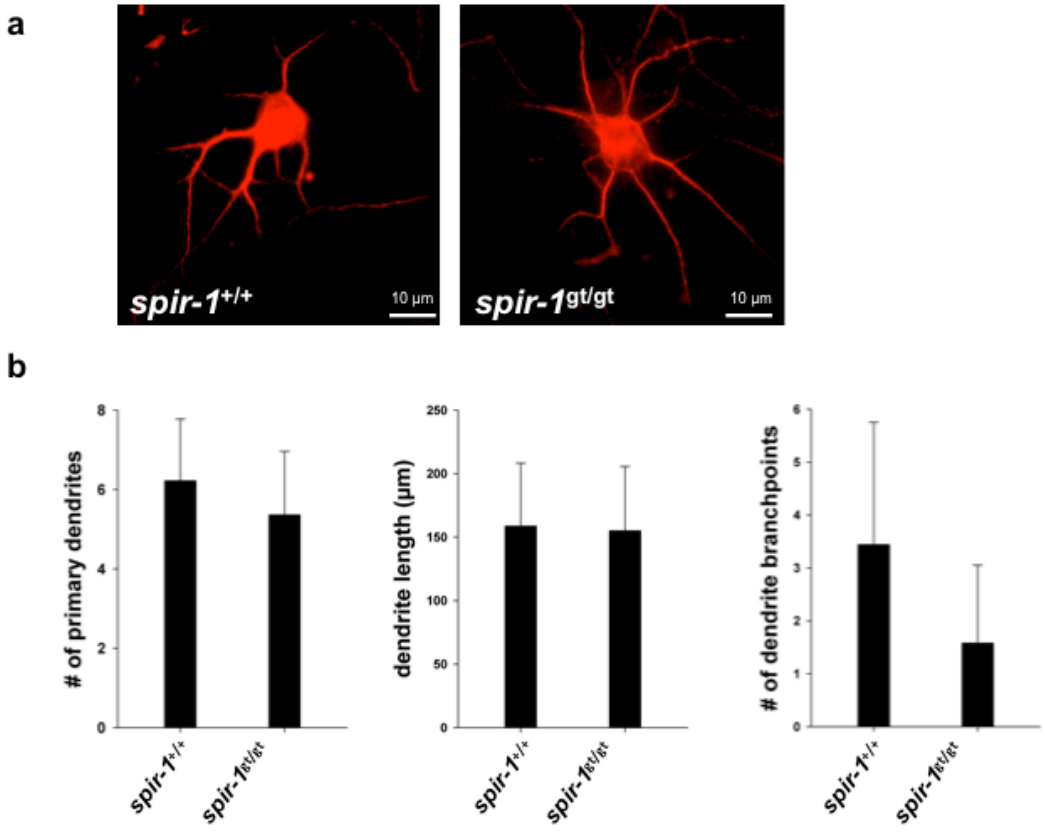

Fig. 2.5 Spir-1 functions in the regulation of dendrite branching during neuronal differentiation
Primary embryonic cortical neurons were isolated from wildtype and Spir-1 deficient embryonic day 14.5 old mouse embryos and differentiated for four days. **a)** Dendritic morphology was revealed by MAP2 immunostaining (red) of wildtype (*spir-1*$^{+/+}$) and Spir-1 deficient (*spir-1*$^{gt/gt}$) cortical neurons. **b)** The average number of dendrites per cell, the average dendrite length per cell and the average number of dendrite branchpoints per cell were determined and presented in bar diagrams. Data are means ± s.d from two different experiments.

2.2.3.2 Impaired dendritic spine formation in Spir-1 deficient neurons

In order to analyze the morphology of individual neurons within the adult brain of Spir-1 deficient neurons, transgenic mice were employed, which express the green fluorescent protein (GFP) under the control of a modified *thy1* promoter region that contains sequences required for neuronal expression but lacks sequences necessary for expression in non-neuronal cells (*thy1*-GFP mice) (Feng *et al*., 2000). Thy1 is a member of an immunoglobulin superfamily and is expressed by projection neurons in many parts of the nervous system, as well as by several non-neuronal cells like thymocytes. It was discovered that individual *thy1*-GFP transgenic mouse lines show a unique transgene expression pattern, with some lines having an intense labeling of small neuronal subsets (Feng *et al*., 2000.) The GFP protein labels neurons in their entirety, including axons, dendrites and dendritic spines. This transgenic mouse line therefore allows the detailed morphological analysis of individual neurons within the mouse neuronal network. *thy1*-GFP-M mice have been provided from Prof. Dr. Frank Bradke (German Center for Neurodegenerative disease (DZNE), Bonn).

thy1-GFP-M mice were first crossed with homozygous *spir-1*$^{gt/gt}$ animals and individuals obtained from the first generation (F1) were then intercrossed. Genotyping was performed by PCR on tail-extracted DNA of the offspring to identify wildtype and Spir-1 deficient mice, which also carry the *thy1*-GFP transgene. 15 µm thick horizontal cryostat sections from *spir-1*$^{+/+}$ / *thy1*-GFP-M and *spir-1*$^{gt/gt}$ / *thy1*-GFP-M mouse brains were prepared and analyzed with a *Leica AF6000LX* imaging system, equipped with a *Leica* DFC350FX camera.

Dendritic spines from neurons in the entorhinal cortex, which is located adjacent to the subiculum, (Fig. 2.6a, LEnt) were quantified. The chosen area displayed a considerable number of GFP-positive dendrites (Fig. 2.6b). A quantitative analysis of GFP positive dendrites revealed a specific reduction of dendritic spines in neurons from Spir-1 deficient mice. Compared to wildtype mice, that exhibit an average of 0.99 dendritic spines per µm dendrite length, Spir-1 deficient mice only show 0.74 spines per µm dendrite length (Fig. 2.6c,d). These experiments were performed together with Isabell Gehring, Master student in Eugen Kerkhoffs laboratory.

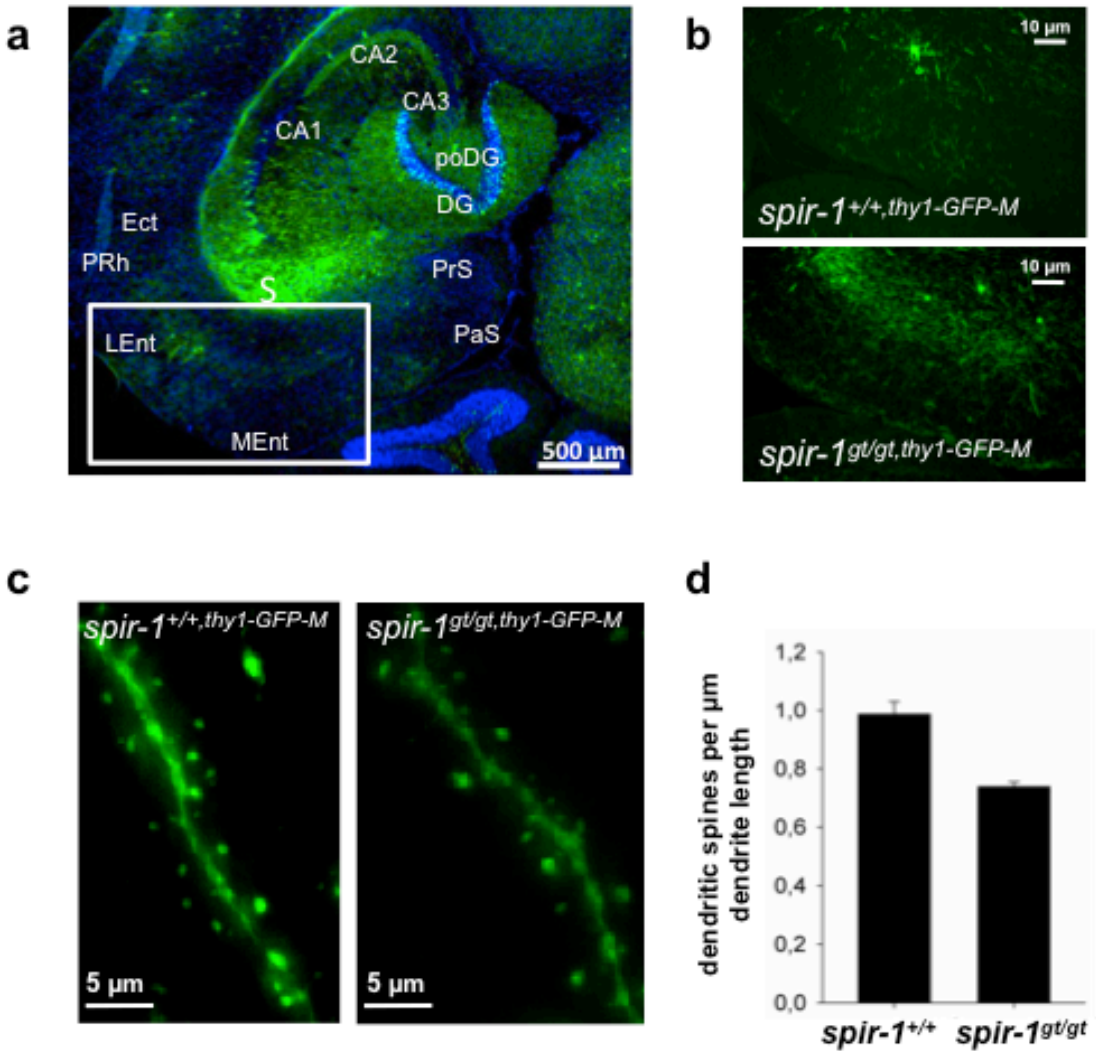

Fig. 2.6 Analysis of dendritic spines in wildtype (*spir-1*$^{+/+}$) and Spir-1 deficient (*spir-1*$^{gt/gt}$) mice, both expressing *thy1*-GFP

a) Horizontal section of a mouse brain illustrates the region of analysis. The area within the framed region indicates the entorhinal cortex, which was assayed for dendritic spine analysis. Nuclei are stained with DAPI (blue). Marked regions: DG, dentate gyrus; poDG, polymorph layer dentate gyrus; Ect, ectorhinal cortex; LEnt, entorhinal cortex, lateral part; MEnt, entorhinal cortex, medial part; PrS, presubiculum; PaS, parasubiculum; PRh, perirhinal cortex; S, subiculum **b)** Overview of GFP positive neurons within the entorhinal cortex of *spir-1*$^{+/+}$ and *spir-1*$^{gt/gt}$ mice. **c)** Representative picture of dendritic spines from wildtype (*spir-1*$^{+/+}$) and Spir-1 depleted mice (*spir-1*$^{gt/gt}$), both expressing the GFP protein. **d)** The average number of dendritic spines per µm dendrite length from *spir-1*$^{+/+}$ and *spir-1*$^{gt/gt}$ mice were quantified and presented in a bar diagram. Data are means ± s.d from two different experiments.

3 Discussion

3.1 Expression patterns of mammalian *spir* genes

3.1.1 *spir-2* shows a broader expression pattern than *spir-1*

Spir proteins belong to the group of WH2 domain containing actin nucleation factors (Quinlan and Kerkhoff, 2008). Spir nucleation activity resides in a cluster of four actin binding WH2 domains in the central part of the protein (Quinlan *et al*., 2005). Although Spir proteins can nucleate actin *in vitro* by themselves, they form a regulatory complex with the distinct actin nucleators of the formin subgroup of formins (Quinlan *et al*., 2007; Pechlivanis *et al*., 2009). Spir protein expression is exclusively restricted to metazoans (Kerkhoff, 2006). The vertebrate genome encodes two *spir* genes, *spir-1* and *spir-2*. The corresponding proteins have an identical structural array and share a high degree of homology (Fig. 1.1) (Pleiser *et al*., 2010). Earlier studies revealed a very restricted expression pattern of the mouse *spir-1* gene (Schumacher *et al*., 2004). Initial *Northern* blot analyses and *in situ* hybridizations showed that mouse *spir-1* is preferentially expressed in the developing nervous system and in the brain. Additionally a weak *spir-1* expression was detected in the spleen (Schumacher *et al*., 2004). To gain more insights into Spir function during mouse development in adult mouse tissues, the yet unknown expression pattern of the mouse *spir-2* gene was analyzed.

To get an initial overview of *spir-2* expression in adult mouse tissues, real-time polymerase chain reaction (PCR) was performed. This study revealed that the mouse *spir-2* gene has a much broader expression pattern than the *spir-1* gene. Highest expression levels of both genes were detected in mouse oocytes and testis. Additionally, a considerable amount of both, *spir-2* and *spir-1* mRNA was found in the brain (telencephalon and cerebellum). Furthermore, a significant expression of *spir-2* was detected within the gastrointestinal tract (stomach, small intestine, large intestine) and kidney. The *spir-1* gene, in contrast, shows only a very weak expression in kidney, stomach and spleen (Fig. 2.1).

These expression data are consistent with those of *Northern* hybridization experiments performed by Jutta Wellmann employing *spir-1* and *spir-2* probes (Pleiser *et al*., 2010). In these experiments two different probes were used to address the question whether splice variants of these genes are expressed in different mouse tissues. Rosales-Nieves *et al*. (2006) proposed splice variants to exist in *Drosophila melanogaster* encoding the isolated N-terminal and C-terminal part of the *Drosophila* Spire protein based on the detection of multiple bands in *Northern* hybridization analyses and DNA sequencing of expressed sequence tags (EST). The data from Pleiser *et al*., however demonstrate that no mouse *spir-2* splice variants exist that

express the isolated N-terminal and C-terminal part of the protein. Both *spir-2* probes (one encoding the Spir-box and FYVE domain (*spir-2*,3') and one encoding the KIND domain and parts of the WH2 cluster (*spir-2*,5')) recognized the same single mRNA (Fig. 3.1). In accordance to previous data from Schumacher *et al*., (2004) both *spir-1* probes (one probe encoding the Spir-box and FYVE domain (*spir-1*,3') and one the KIND domain and parts of the WH2 cluster (*spir-1*,5')) detected two major bands. (Fig. 3.1). Likewise, this *Northern* hybridization analysis showed that *spir-2* is much broader expressed than *spir-1*. A substantial expression of *spir-2* was also detected throughout the gastrointestinal tract (stomach, small and large intestine), the brain and testis. A weak expression of *spir-2* was found in kidney (Fig. 3.1, left panels). The *spir-1* gene is highly expressed in brain; a minor expression is detected in testis, spleen and kidney (Fig. 3.1, right panels).

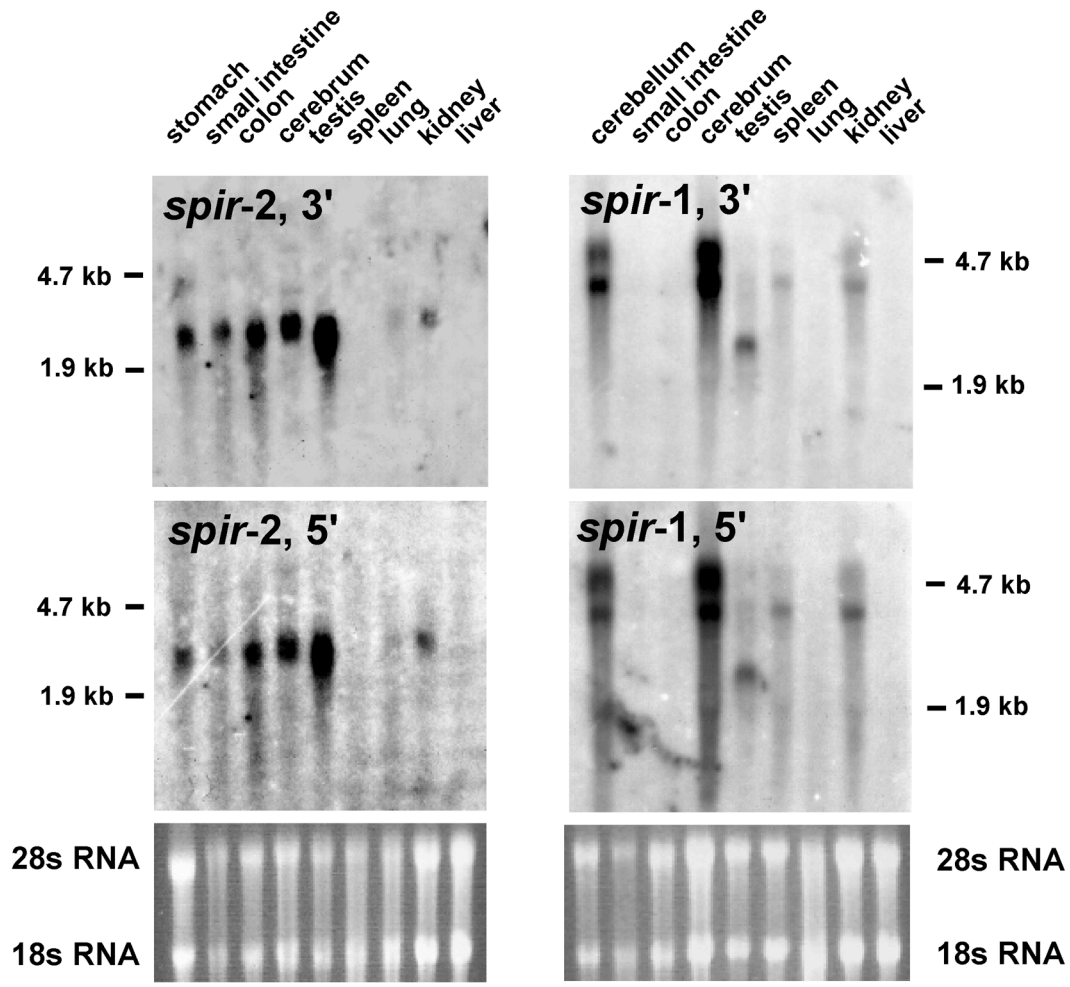

Fig. 3.1 *Northern* hybridization analysis of *spir-1* and *spir-2* gene expression (figure from Pleiser *et al.*, 2010)

Total mouse RNA of the indicated tissues were separated on a formaldehyde-agarose gel and blotted onto a Duralon UV membrane. (α-^{32}P)dCTP labeled probes were employed, which encode fragments of the 5' and 3' coding region of *spir-1* and *spir-2*, respectively (*spir-2*,3'; *spir-2*,5'; *spir-1*,3'; *spir-1*,5'). Size of ribosomal RNAs 4.7 and 1.9 are marked. Ethidiumbromide stained 28s and 18s RNAs are shown as loading control.

3.1.2 *spir* expression in the mouse oocyte

The expression of mammalian *spir-1* and *spir-2* genes in adult mouse tissues has been studied by real-time PCR analysis. Highest levels of both genes were detected in mouse oocytes (Fig. 2.1). Very recently both *spir* genes were described to cooperate with the mouse formin-2 protein to drive asymmetric oocyte division (Pfender *et al*., 2011). Asymmetric meiotic division requires two steps, the asymmetric spindle positioning and polar body extrusion. It was found that both Spir proteins act redundantly in mediating asymmetric spindle positioning by assembling the cytoplasmic actin meshwork (Pfender *et al*., 2011). Confocal live cell imaging of mouse oocytes revealed that the asymmetric positioning of the spindle failed when co-depleting *spir-1* and *spir-2* with siRNA (Pfender *et al*., 2011). A cytoplasmic actin network was described before, that provides the substrate for myosin dependent spindle movement and is therefore required for asymmetric spindle positioning (Simerly *et al*., 1998; Schuh and Ellenberg, 2008; Azoury *et al*., 2008). In *spir-1* and *spir-2* co-depleted mouse oocytes this cytoplasmic actin mesh was greatly reduced (Pfender *et al*., 2011). Furthermore it was shown, that both proteins colocalized at the cleavage furrow during polar body extrusion, which was found to be dependent on Spir function (Pfender *et al*., 2011). Only 30% of *spir-1* and *spir-2* co-depleted oocytes extruded a polar body and 68% failed to assemble a cleavage furrow upon anaphase onset (Pfender *et al*., 2011).

Spir proteins cooperate with the distinct actin nucleators of the formin subgroup of formins (*Drosophila melanogaster* cappuccino protein and its two vertebrate homologues formin-1 and formin-2) (Quinlan *et al*., 2007; Pechlivanis *et al*., 2009). The *Drosophila spire* and *cappuccino* mutants were identified in the same genetic screen and have an identical phenotype (Manseau and Schupbach, 1989; Wellington *et al*., 1999). It was later found that both proteins directly interact with each other and regulate a common actin meshwork in the Drosophila oocyte, which suppresses premature cytoplasmic streaming (Dahlgaard *et al*., 2007; Quinlan *et al*., 2007). The data from Pfender *et al*. (2011) demonstrate that also mouse Spir proteins, Spir-1 and Spir-2, cooperate with the Cappuccino homolog formin-2 (Fmn-2) protein in regulating a similar actin meshwork in mouse oocytes. Both Spir-1 and Spir-2 colocalized with formin-2 at the oocyte surface, in the cytoplasm and in the cleavage furrow. Moreover, the co-overexpression of both Spir proteins with Fmn-2 led to an increase of 198% of the density of the actin network in oocytes, whereas overexpression of Spir-1/Spir-2 or formin-2 alone only caused an increase of 29% or 69%, respectively. Further, in these studies it could be demonstrated that both nucleators depend on each other to assemble F-actin and act in a functional unit. Neither the overexpression of Fmn-2 in *spir-1*/*spir-2* co-depleted oocytes, nor overexpression of both Spir proteins in oocytes derived from *fmn-2*$^{-/-}$ mice increased

the density of the actin network (Pfender *et al*., 2011). These data imply that both actin nucleators interact in a cooperative manner to assemble the actin meshwork in mouse oocytes. Spir/formin cooperation is therefore considered to be a major regulatory function in mammalian oocyte maturation. Since the mechanism of asymmetric oocyte division is likely to be conserved between humans and mice it would be important to consider defects in any of these three proteins to cause unexplained infertility in humans (Ryley *et al*., 2005; Pfender *et al*., 2011). Consistently, hypofertility was identified as a major phenotype of formin-2 deficient mice (Leader *et al*., 2002).

3.1.3 *spir* expression in the nervous system

The real-time PCR analysis revealed, next to the high expression of both *spir* genes in oocytes, also a considerable amount of *spir-2* as well as *spir-1* mRNA in the mouse brain. Previous studies already revealed high *spir-1* expression in the entire developing nervous system (forebrain, midbrain, neural tube and the trigeminal ganglion (Schumacher *et al*., 2004).

In situ hybridizations were performed to determine the spatial and temporal expression of the *spir-2* gene during mouse embryogenesis. It was found that *spir-2* expression is already evident at embryonic day 11.5 (E11.5) throughout the central nervous system and that this intense expression remained strong until late stages of embryonic development (embryonic day 17.5) (Fig. 2.2a). In the peripheral nervous system *spir-2* mRNA was detected in dorsal root ganglia and the trigeminal ganglion. (Fig. 2.2a). Although there is a high degree of overlap (overlapping expression patterns of both *spir* genes in forebrain with a pronounced expression in the cerebral cortex, midbrain and the trigeminal ganglion), specific differences in the expression patterns were identified in the neural tube (Fig. 2.2c) (Pleiser *et al*., 2010).

At embryonic day 11.5 (E11.5) *spir-2* is expressed in the mantle layer, the ventral horn and in dorsal root ganglia whereas strongest *spir-1* expression is observed in the ventricular zone and the dorsal horn of the neural tube. It is interesting to note that at this stage of development the *spir-2* and *spir-1* expression is clearly distinct from each other in the neural tube; areas that express the *spir-2* gene do not express *spir-1* and vice versa (Fig. 2.2c, left panels). At later stages of development both *spir* genes show an evenly and identical expression throughout the neural tube (Fig. 2.2c, right panels) (Pleiser *et al*., 2010). The speckled expression indicates a cell type specific and presumably neuronal expression pattern of both genes. Further these data demonstrate that at early stages of neural tube development *spir* gene expression is tightly spatially regulated. Whereas at E11.5 both *spir* gens are differentially expressed and might therefore act in different cellular processes later in

development *spir-2* and *spir-1* expression overlaps. This indicates a redundant function of both *spir* genes at that time point of development (Pleiser *et al*. 2010).
In the adult nervous system the separation of *spir-1* and *spir-2* gene expression is even more pronounced. Although both mouse *spir* genes are highly expressed in the brain as indicated by the real-time PCR analyses (Fig. 2.1), there is only a minor overlap in their expression pattern, which is mainly restricted to the Purkinje cell and the granule cells of the cerebellum, the cortex and the thalamus. The hippocampal neurons only express the *spir-1* gene, whereas *spir-2* expression is high in the external and central nucleus of the inferior colliculus as well as the intercollicular nucleus and the external capsule, where no *spir-1* expression is detectable. In contrast, *spir-1* expression is observed in the lateral septal nucleus and the anterodorsal nucleus (Fig. 2.3a) (Pleiser *et al*., 2010).
Because of the high structural similarity of the two Spir proteins (Fig. 1.1), one can speculate that the proteins may fulfill the same biological function in the different neuronal cells and the fact that in most cases only one of the genes is expressed may implicate that the cellular Spir concentration is tightly regulated.

3.1.4 *spir-2* expression in the intestine and testis

To define the cellular nature of *spir-2* expression in the mouse intestine and testis, *in situ* hybridization analysis was performed. It was found that first expression of *spir-2* in the developing intestine is detected at embryonic day 17.5 (Fig. 2.2d, right panel) (Pleiser *et al*., 2010). No staining could be observed at embryonic day 15.5 (Fig. 2.2 a), a stage in mouse development at which the epithelial monolayer and the villi are formed (Stappenbeck *et al*., 1998). This indicates that Spir-2 function is not needed for the early steps of intestinal development. Since however the intestinal morphogenesis is not completed until the end of the third postnatal week, Spir-2 could function in later steps of development (Pleiser *et al*., 2010). Consistently, *in situ* hybridization analysis of the adult mouse digestive tract revealed *spir-2* expression in intestinal epithelial cells along villi and crypts (Fig. 2.3c, left panels) (Pleiser *et al*., 2010).
In situ hybridization analysis of the adult mouse testis revealed *spir-2* mRNA expression in seminiferous tubules, with a strong staining in spermatocytes. In spermatogonia no *spir-2* expression was observed (Fig. 2.3, right panels) (Pleiser *et al*., 2010). The immature germ cells are located at the outer edge of the seminiferous tubules next to the basal lamina. The testosterone secreting Leydig cells, which are located between the seminiferous tubules and large Sertolli cells, which extend from the basal lamina to the lumen of the seminiferous tubules also do not express *spir-2*. The *spir-2* gene expression in testis is therefore restricted to spermatocytes. These

cells develop from the spermatogonia stem cells in a differentiation step and undergo two meiotic divisions (Pleiser *et al*., 2010).

3.1.5 Summary

Spir proteins are only expressed in metazoans (Kerkhoff *et al*., 2006). The restricted expression of the *spir-1* gene could lead to the assumption, that the function of this novel actin nucleator might be needed only for a subset of highly specialized cells. Within the scope of this work it was shown that the second mammalian *spir* gene, *spir-2*, has a broader expression pattern than *spir-1* and is highly expressed in tissues, which lack or have very low expression of the *spir-1* gene. A partial redundancy of the proteins can be hypothesized during brain development and in the adult cerebellum since in these tissues both *spir* genes are highly expressed. A redundant function of Spir-1 and Spir-2 proteins has been already documented in the mouse oocyte (Pfender *et al*., 2011). Thus, Spir functions in a diversity of mammalian cells, including neuronal cells, epithelial cells of the digestive tract, spermatocytes and oocytes proving, that both Spir proteins seem to act in a diversity of cellular processes (Pleiser *et al*., 2010).

3.2 Mouse genetic analyses of Spir-1 function

Although substantial knowledge about the biochemical function of Spir proteins in the process of actin nucleation has been raised (Kerkhoff, 2011), the developmental and cell biological functions of Spir proteins are not well understood. A mouse genetic approach was chosen to address the function of Spir proteins in the mouse nervous system, as its major tissue of expression (besides oocytes).

Because of the predominant expression of *spir-1* in neuronal cells, the clear distinction from *spir-2* expression and the fact that organisms such as the worm *C.elegans* can develop and operate a functional nervous system without expressing any Spir or formin subfamily protein, it was assumed that a conventional non conditional knock-out should generate viable mice to study Spir-1 function in the nervous system.

Thus, Spir-1 deficient mice were generated by the Texas A&M Institute for Genomic Medicine (TIGM) using a gene trap approach. The gene trap disrupts *spir-1* mRNA at sequences encoding a region immediately downstream the N-terminal Spir KIND domain (Fig. 2.4a). Two heterozygous *spir-1*$^{gt/+}$ males and two heterozygous *spir-1*$^{gt/+}$ females were handed out by TIGM and a breeding colony was established during this work. The insertion of the gene trap cassette was confirmed by reverse-transcription PCR (RT-PCR) of brain RNA preparations from wildtype and homozygous *spir-1*$^{gt/gt}$ littermates (Fig. 2.4b). The absence of Spir-1 protein expression in *spir-1* homozygous *spir-1*$^{gt/gt}$ mice was proven by Western blot using a rabbit polyclonal anti-Spir-1 antibody raised against a C-terminal peptide of the Spir-1 protein (Fig. 2.4c).

Initial phenotyping of Spir-1 deficient mice didn't reveal any macroscopic or microscopic abnormalities. The fertility of Spir-1 deficient mice was of special interest since knock-out mice of the Spir interaction partner Fmn-2 exhibit a female hypofertility, due to a function of Fmn-2 in positioning the metaphase spindle during meiosis I in oocyte maturation (Leader *et al*., 2002.). In this study no reduced fertility could be observed in *spir-1*$^{gt/gt}$ females, though. This is however in accordance to the data from Pfender *et al*. (2011), where it was found that both mammalian *spir* genes had to be knocked-down in order to generate the formin-2 knock-out phenotype in the oocyte. Due to the fact that Spir proteins act redundantly in the oocyte (Pfender *et al*., 2011), Spir-1/Spir-2 double knock-out mice should be generated and investigated for female infertility.

3.2.1 Function of Spir-1 in neuronal differentiation

Because of the selective expression of the *spir-1* gene in neuronal cells of the developing and adult mouse nervous system, it was analyzed whether Spir-1 has a function in the morphogenesis of the neuronal network. Initial experiments employing primary cortical neurons of *spir-1*$^{gt/gt}$ embryonic day 14.5 embryos and wildtype littermates revealed a reduction of dendrite branchpoints in cortical neurons from Spir-1 deficient mice (Fig. 2.5) and are the first description of a neuronal Spir-1 function. The underlying mechanisms however still have to be elucidated.

A basic model system of neuronal differentiation has been well established in cultured hippocampal neurons (Craig and Banker, 1994; Kaech and Banker, 2006). These neurons maintain their intrinsic ability to establish a single axon and several dendrites after culturing them on a two-dimensional substrate (Dotti *et al*., 1988). Shortly after plating, the neurons attach to their substrate (i.e polylysine and laminin) as round spheres, which are surrounded by lamellipodia and filopodia. This stadium is referred to as stage 1 (Tahirovic and Bradke, 2009; Neukirchen and Bradke, 2011). 12-24 (stage 2) hours later the spheres develop several short processes, the minor neurites that are covered with dynamic growth cones at their tips. At that time point the neurons are still unpolarized, but show characteristic alternations of growth and retraction. Neuronal polarity is established when one of these minor neurites rapidly grows to become the axon. This event occurs 24-48 hours post plating (stage 3). The remaining minor neurites eventually develop into dendrites (> 72 hours, stage 4) and after one week in culture (stage 5) a functional polarization of axons and dendrites with the formation of synapses takes place. Subsequently, dendritic spines are formed two weeks after plating (stage 6) (Dotti *et al*., 1988; Craig and Banker, 1994; Tahirovic and Bradke, 2009).

Cytoskeletal dynamics play a crucial role for the establishment of neuronal polarity (Neukirchen and Bradke, 2011). The determining event for neuronal polarization is the formation of the axon. The growth cone of the future axon in unpolarized cells shows a decreased stability of its actin cytoskeleton. It becomes more dynamic and less dense, while the actin cytoskeleton of the growth cones of the remaining minor neurites remains less dynamic and retains a dense meshwork (Bradke and Dotti, 1999). It is proposed that this instability of the actin cytoskeleton in the growth cone of the future axon allows microtubules to protrude to the peripheral region of the growth cone and thus, to stimulate axon extension (Bradke and Dotti, 1999). Accordingly, the more condensed and less dynamic actin cytoskeleton in the growth cone of the remaining minor neurites hinders microtubules to advance to the peripheral region of the growth cone (Bradke and Dotti, 1999). Moreover, microtubules are more stable along the shaft of the future axon in comparison to the minor neurites (Witte and Bradke, 2008).

Dendrites differ from axons in many important aspects, such as length, diameter, growth rate and molecular composition (Craig and Banker, 1994). They extend in a defined direction and increase in diameter as they form branches at defined intervals. As dendrites elaborate, they generate highly specialized structures, the dendritic spines, which are the main excitatory synapses in the mammalian brain (Gao *et al*., 1999; Lee and Luo, 1999). When dendrites extend away from their soma into their target field, most neurons form extensive dendritic branches (Scott and Luo, 2001). This process can be generated by two distinct mechanisms. The predominant observed mechanism in cultured neurons is the splitting of the growth cone under certain conditions (Bray, 1973). The second mechanism, which is supposed to be the predominant one in more physiological conditions, is the emergence of branches from the side of established dendritic shafts and is called interstitial branching (Dailey and Smith, 1996). Live cell imaging analysis of pyramidal neurons from developing rat hippocampal slices revealed, that branches appear in form of a single filopodium and some develop then into growth cone like structures which extend and become stable branches (Dailey and Smith, 1996).

To gain further insight of Spir-1 function in neuronal differentiation, live cell imaging fluorescence microscopy experiments should be performed to monitor the actin and microtubule cytoskeleton during neuronal differentiation. Cultured primary hippocampal neurons could be transfected or microinjected with expression vectors directing the expression of green fluorescent protein tagged Spir-1 as well as vectors expressing red fluorescent tagged proteins to monitor the actin and microtubule cytoskeleton. It would be interesting to focus on the localization of Spir vesicles during the process of neuronal differentiation.

3.2.2 Function of Spir-1 in dendritic spine formation

The selective expression of *spir-1* in neuronal cells as well as the cell culture data showing a reduced number of dendrite branches in Spir-1 deficient cultured primary cortical neurons indicate a function of Spir-1 in the morphogenesis of the neuronal network. In order to analyze the morphology of neurons within the adult brain of Spir-1 deficient mice, a transgenic mouse line (*thy1*-GFP-M) was employed that expresses the green fluorescent protein (GFP) in individual neurons of the cortex and hippocampus (Feng *et al*., 2000), areas where also *spir-1* expression was detected. The GFP protein labels neurons in their entirety, including axons, nerve terminals dendrites and dendritic spines. Spir-1 deficient *spir-1*$^{gt/gt}$ / *thy1*-GFP-M mice have been generated during this work and 15 µm thick brain cryostat sections of wildtype and Spir-1 deficient mice, both expressing the GFP protein, were prepared. *In situ* hybridization analysis in the adult mouse brain has previously shown a substantial expression of the *spir-1* gene in the entorhinal cortex. The entorhinal cortex is the principal interface between the hippocampal formation and the neocortex (Canto *et al*., 2008). It is subdivided into two areas, the lateral entorhinal area (LEA) and the medial entorhinal area (MEA), which specifically connect functionally different sets of cortical and subcortical areas in the brain (Canto *et al*., 2008). Dendritic spines of GFP positive neurons within the entorhinal cortex were quantified. It was found that Spir-1 deficient mice exhibit a considerable reduction of dendritic spines in the entorhinal cortex as compared to wildtype mice (Fig. 2.6 c,d).

Dendritic spine growth as well as new spine formation is strongly correlated to AMPA receptor trafficking. It was shown that recycling endosomes, which are located within or at the base of dendritic spines, contain pool of AMPA receptors. These recycling endosomes are rapidly mobilized during long-term potentiation and AMPA receptors are delivered to the plasma membrane and finally inserted (Ehlers, 2000; Park *et al*., 2006). Disruption of the trafficking of recycling endosomes was shown to block activity-dependant AMPA receptor insertion, spine growth and new spine formation (Park *et al*., 2004; Park *et al*., 2006).

The very high expression of *spir-1* in the hippocampus and entorhinal cortex and its close relation to Rab11 regulated vesicle transport processes (Kerkhoff *et al*., 2001) (Schuh, 2011) suggest a role for Spir-1 in receptor recycling effects on long-term potentiation (LTP) and memory. Rab11 is localized at the trans-Golgi network, post-Golgi vesicles and the recycling endosome and functions in exocytosis and recycling processes of cell membrane proteins (Chen *et al*., 1998; Sönnichsen *et al*., 2000; Stenmark, 2009). Together with its effector, the actin motor protein myosin Vb, Rab11 functions in AMPA receptor trafficking necessary for postsynaptic plasticity (Wang *et al*., 2008). Disruption of myosin Vb abolishes LTP induced exocytosis from recycling endosomes and prevents both, AMPA receptor insertion and spine growth

(Wang *et al*., 2008). Spir-1 colocalizes with Rab11 when coexpressed in mammalian fibroblasts (Kerkhoff *et al*., 2001) and Spir-1, -2, formin-2, Rab11 and myosin Vb were recently shown to function together in actin dependent long range vesicle transport processes in mouse oocytes (Schuh, 2011). It therefore could be assumed that Spir-1 also plays a role in AMPA recycling processes. Given that in Spir-1 depleted neurons the trafficking of recycling endosomes is impaired, AMPA receptor recycling could be blocked, thus explaining the reduced number of dendritic spines in Spir-1 deficient neurons.

To manifest this assumption, the exocytosis of AMPA receptors from recycling endosomes could be monitored by live cell imaging of wildtype and Spir-1 depleted hippocampal neurons, transfected or microinjected with a pHlourin tagged GluR1 subunit of the AMPA receptor. pHlourins are pH sensitive mutants of the green fluorescent protein. The fluorescent signal of pHlourin increases significantly when the pH changes from acidic to neutral. Since the pH in the lumen of trafficking vesicles is slightly acidic (< 6.0) an increase of pHlourin fluorescence indicates plasma membrane insertion of the pHlourin tagged GluR1 (Miesenböck *et al*., 1998).

The trafficking of AMPA receptors is strongly linked to learning-related plasticity at excitatory synapses in the mammalian brain. To further substantiate the potential role of Spir-1 function in learning and memory processes, behavior tests like open field, Y-Maze, elevated plus maze and Morris Water Maze with the Spir-1 depleted mice should be conducted.

All together these data give new insights into the mechanisms how cytoskeletal functions structure the mammalian neuronal network and are the first description of a neuronal function of the Spir-1 actin nucleator.

4 Materials and Methods

4.1 Materials

4.1.1 Disposable materials

Article	Order Number	Company
Sterilization tape (180°C)	STKH	distributed by A. Hartenstein Laborbedarf
Autoclave indicator tape (120°C)	STKD	distributed by A. Hartenstein Laborbedarf
Blotting papers Grade 3 MM Chr	3030.917	Whatman
Cell culture dish (100 x 20 mm)	664160	Greiner Bio-One
Cell culture dish (60 x 15 mm)	150288	Thermo Scientific, Nunc
Cell culture plate (24- well)	83.1836	Sarstedt
Cell culture plate (6- well)	657160	Greiner Bio-One
Conical reaction tubes (15 ml)	188271	Greiner Bio-One
Conical reaction tubes (50 ml)	227261	Greiner Bio-One
Embedding cassette	E478.1	Carl-Roth
pH indicator sticks (pH 4.5-10.0)	92120	Machery-Nagel
Microscope cover glasses (12 mm diameter)	0111520	Marienfeld Laboratory Glassware
Microscope cover glasses (15 mm diameter)	0111550	Marienfeld Laboratory Glassware
Microscope cover glasses (24 x 50 mm)	0101222	Marienfeld Laboratory Glassware
Microscope slides SuperFrost® Plus	J1800AMNZ	Menzel, Thermo Scientific
Nitrocellulose transfer membrane, PROTRAN® BA85, 0.45 µM pore size	10401196	Whatman
Parafilm® “M” Laboratory	PM-996	Pechiney Plastic

Film		Packaging
Pasteur pipettes	PP07	distributed by A. Hartenstein Laborbedarf
PCR-tubes (0.2 ml)	PCR-0208-CP-C	Axygen, distributed by Abimed
Petri dishes (94 x 16 mm)	PP90	distributed by A. Hartenstein Laborbedarf
Pipette tips, white (0.5-10 µl)	T-300	Axygen, distributed by Abimed
Pipette tips, blue (100-1000 µl)	T-1000-B	Axygen, distributed by Abimed
Pipette tips, yellow (2-20 µl) and (20-200 µl)	70.760.002	Sarstedt
Reaction tubes (1.5ml)	RK1G	distributed by A. Hartenstein Laborbedarf
Reaction tubes (2.0ml)	RK2G	distributed by A. Hartenstein Laborbedarf
Scalpel	147222	Megro
Syringe (1 ml) with needle 0.45 x 10 mm	300015	Becton-Dickinson
Syringe (10 ml)	4606108V	Braun
Syringe (50 ml)	22050	Dispomed
Syringe filter (0.2 µm)	17597	Sartorius Stedim Biotech
TissueRuptor disposable probes	990890	Qiagen
X-ray film	47410 08379	FujiFilm

4.1.2 Chemicals and Reagents

Article	Order Number	Company
Acetic acid	3738.1	Carl-Roth
Acetic Anhydride	CP28.1	Carl-Roth
Acrylamide (30%)/ Bisacrylamide (0,8%) (37.5:1)	3029.1	Carl-Roth
Agarose, UltraPure™	15510-027	Invitrogen
Ammonium persulfate	A3678	Sigma-Aldrich
BCP, phase separation reagent	BP151	MRC Molecular Research Center, Inc.
Beta-Mercaptoethanol	4227.3	Carl-Roth
BioTherm buffer, 10 x, 15mM $MgCl_2$	GC-002-006	Genecraft
Blocking Reagent	11 096 176 001	Roche Diagnostics
BM Purple	11 442 074 001	Roche Diagnostics
Bovine serum albumin, Cohn V fraction	A4503	Sigma-Aldrich
Bromophenol blue	A512.1	Carl-Roth
CHAPS	1479.1	Carl-Roth
Citric acid monohydrate	3958.2	Carl-Roth
DAPI	6335.1	Carl-Roth
Diethyl Pyrocarbonate (DEPC)	D5758	Sigma-Aldrich
dNTP set, 100 mM	GC-013-001	Genecraft
EDTA	E5134	Sigma-Aldrich
Eosin Y solution, 0.5% aqueous	X883.1	Carl-Roth
Ethanol >99.8%, p.a.	9065.2	Carl-Roth
Ethanol denatured (+1% Mek)	K928.1	Carl-Roth
Ethidiumbromide	HP46.1	Carl-Roth
Formamide	6749.2	Carl-Roth
Formamide deionized	P040.1	Carl-Roth
Glycerol	3783.1	Carl-Roth
Glycine	G7126	Sigma-Aldrich
Heparin sodium salt	H3393	Sigma-Aldrich

Isopropanol	A0900	AppliChem
Ketamine	Available on prescription Approval. No. 9089.01	WDT
Levamisole hydrochloride	L9756	Sigma-Aldrich
Magnesium chloride hexahydrate	2189.2	Carl-Roth
Maleic acid >99%	3538.1	Carl-Roth
Mayers hemalaum solution	T865.1	Carl-Roth
Methanol 99.9%	4627.2	Carl-Roth
Milk powder, blotting grade	T145.2	Carl-Roth
Mowiol	475904	Calbiochem
Paraformaldehyde	0335.1	Carl-Roth
Paraplast®Plus	X881.1	Carl-Roth
PBS buffer (10X Dulbecco's) – powder	A0965	AppliChem
Ponceau S	P3504	Sigma-Aldrich
Salmon sperm DNA	201190	Agilent Technologies
Sodium chloride	S3014	Sigma-Aldrich
Sodium citrate tribasic dihydrate	S4641	Sigma-Aldrich
Sodium dodecyl sulfate (SDS)	L4390	Sigma-Aldrich
Sodium hydroxide pellets	106462	Merck
TEMED	T9281	Sigma-Aldrich
Trichlormethane/ Chloroform	3313.1	Carl-Roth
Triethanolamine	6300.1	Carl-Roth
Tris-(hydroxymethyl)-aminomethane	A1086	AppliChem
Triton X 100	3051.3	Carl-Roth
Trizol® Reagent	15596026	Invitrogen
t-RNA	10 109 517 001	Roche Diagnostics
Tween 20	A1389	AppliChem
Xylazine	Available on prescription Approval No. 3100265.00	Serumwerk Bernburg AG
Xylol >98%, for Histology	9713.3	Carl-Roth

4.1.3 Cell Culture Media, Reagents and Supplements

Article	Order Number	Company
B-27 supplement	17504044	Invitrogen, Gibco
Dulbeccos's Phosphate Buffered Saline 1X	14190094	Invitrogen, Gibco
Fetal bovine serum, Fetalclone III	SH30109.03	Thermo Scientific, HyClone
HBSS	14025050	Invitrogen, Gibco
Horse serum	26050088	Invitrogen, Gibco
Laminin	L2020	Sigma-Aldrich
L-Glutamine	25030024	Invitrogen, Gibco
Neurobasal Medium	21103049	Invitrogen, Gibco
Penicillin/Streptomycin	15140122	Invitrogen, Gibco
Poly-D-Lysine	P7280	Sigma-Aldrich

4.1.4 Antibodies

Primary Antibodies

Article	Species/Clonality	Order Number	Company
anti-Digoxigenin-AP	sheep, polyclonal	11093274910	Roche diagnostics
anti-MAP2 (HM-2)	mouse, monoclonal	ab11267	Abcam
anti-Spir-1 (SA2133)	rabbit, monoclonal		made by AG Kerkhoff

Secondary Antibodies

Article	Species	Order Number	Company
Anti-mouse Fluorescein (FITC) IgG (H+L)	donkey	715-095-151	Jackson Immuno Research Laboratories
Anti-mouse Rhodamine (TRITC) IgG (H+L)	donkey	715-025-151	Jackson Immuno Research Laboratories
ECL™ Anti-Rabbit HRP IgG	donkey	NA9310V	GE Healthcare

4.1.5 Enzymes

Article	Order Number	Company
*Bam*HI	R0136L	New England Biolabs
Proteinase K (genotyping)	7528.1	Carl-Roth
Proteinase K (in situ hybridization)	03 115 836 001	Roche Diagnostics
RNase A	19101	Qiagen
Taq-Polymerase (BioTherm) 5 units/ µl	GC-002-0500	Genecraft

4.1.6 Kits

Article	Order Number	Company
Amersham™ECL™ Western Blotting Analysis System	RPN2109	GE Healthcare
DIG RNA labeling Kit	11175025910	Roche Diagnostics
LightCycler 480 Green I Master	04707516001	Roche Diagnostics
NucleoSpin® Extract II	740609.50	Machery-Nagel
QuantiTect Reverse Transcription Kit	205310	Qiagen

4.1.7 Molecular Weight Markers

Protein Standard	**Order Number**	**Company**	**Fragment sizes**
Precision Plus Protein Standard Dual Color	161-0374	Bio-Rad	in kD: 250, 150, 100, 75, 50, 37, 25, 20, 15, 10
DNA Standards			
1 kb DNA-ladder	25-2030	Peqlab	in bp: 10000, 8000, 6000, 5000, 4000, 3500, 3000, 2500, 2000, 1500, **1000**, 750, 500, 250
100 bp DNA-ladder	25-2010	Peqlab	in bp: 1000, 900, 800, 700, 600, **500**, 400, 300, 200, 100

4.1.8 Oligonucleotides

All oligonucleotides were synthesized by eurofins MWG operon

Primer name	**Sequence (5'-3')**
mm-spir-1-forward	AGC TCT GCT TCT GTT GCC GA
mm-spir-1-reverse	CTC GAA CAG CTT TCC CCC CT
mm-spir-2-forward	AAA TCA AGC AGG AGC GGA GG
mm-spir-2-reverse	GGT GGG GGC TTT GAG CAH GA
OST416113-forward	GCA TGA CTC TTT GGA GAG CAT TAG C
OST416113-reverse	AGG CTA CAA GAA CTG GTC TCC AAG C
LTR-reverse	ATA AAC CCT CTT GCA GTT GCA TC
0IMR0872-forward	AAG TTC ATC TGC ACC ACC G
0IMR1416-reverse	TCC TTG AAG AAG ATG GTG CG
mm-spir-1-KIND-KIND-forward	ATG GCT TGA AGG AAA ACG AA
mm-spir-1-KIND-KIND-reverse	GAC TCA GTT GGG AGG TGA GC
mm-spir-1-KIND-WH2-forward	CCG GTC CTA TCA GGA CGT TA
mm-spir1-KIND-WH2-reverse	ATG GGC AGA GGG TTG TAC TG
beta-microglobulin-forward	ATG GGA AGC CGA ACA TAC TG
beta-microglobulin-reverse	CAG TCT CAG TGG GGG TGA AT

Following primer sets were used:

Primer sets	Annealing temperature	Product size	Purpose/ Annotation
mm-spir-1-forward mm-spir-1-reverse	59°C	187 bp	Real-time PCR
mm-spir-2-forward mm-spir-2-reverse	59°C	194 bp	Real-time PCR
beta-microglobulin-forward beta-microglobulin-reverse	59°C	140 bp	Real-time PCR
mm-spir-1-KIND-KIND-forward mm-spir-1-KIND-KIND-reverse	60°C	220 bp	referred to as primer set 1 in fig. 2.4
mm-spir-1-KIND-WH2-forward mm-spir-1-KIND-WH2-reverse	60°C	318 bp	referred to as primer set 2 in fig. 2.4
OST416113-forward OST416113-reverse	61°C	269 bp	Genotyping / amplifying wildtype allele
OST416113-forward LTR-reverse	61°C	142 bp	Genotyping / amplifying mutant allele of *spir-1*$^{gt/gt}$ mice
0IMR0872-forward 0IMR1416-reverse	60°C	173 bp	Genotyping / amplifying *thy1*-GFP transgene as recommended by the Jackson laboratory

4.1.9 Mouse lines

Line	Company
CD1	Charles River
spir-1$^{gt/+}$	Texas A&M Institute for Genomic Medicine
thy1-GFP-M	kindly provided from Prof. Dr. Frank Bradke, DZNE, Bonn

4.1.10 Solutions and Buffers

4.1.10.1 General buffers

1M Citric acid monohydrate (50 ml)
10.5 g of citric acid monohydrate were dissolved in 50 ml of Millipore-H_2O. The solution was autoclaved and stored at room temperature.

DEPC-H_2O (1 l)
1 ml of DEPC was added to 1 l of Millipore-H_2O. The mixture was stirred until DEPC was fully dissolved. Solution was autoclaved to destroy the DEPC and stored at room temperature.

0.5 M EDTA (disodium salt dihydrate) pH 8.0 (1 l)
186.1 g of EDTA were added to 800 ml of Millipore-H_2O. NaOH pellets (approximately 20 g) were added while stirring to bring the pH to 8.0. The volume was adjusted to 1 l. Solution was autoclaved and stored at room temperature.

0.5 M EDTA (disodium salt dihydrate) /DEPC pH 8.0 (1 l)
186.1 g of EDTA were added to 800 ml of Millipore-H_2O. NaOH pellets (approximately 20 g) were added while stirring to bring the pH to 8.0. 1 ml of DEPC was added and the volume was adjusted to 1 l. The Solution was stirred until the DEPC was fully dissolved, autoclaved and stored at room temperature.

4 M LiCl/DEPC (50 ml)
8.5 g of lithium chloride were dissolved in 50 ml of Millipore-H_2O. 50 µl of DEPC were added and the solution was stirred until the DEPC was fully dissolved. The solution was autoclaved and stored at room temperature.

1 M $MgCl_2$ hexahydrate (500 ml)
101,7 g of $MgCl_2$ were dissolved in 1 l of Millipore-H O. The solution was autoclaved and stored at room temperature.

Mowiol solution (100 ml)
15% (w/v) mowiol, 30% (v/v) glycerol, 2.25% (w/v) N-propyl gallate
15 g of mowiol were added to 70 ml of Millipore-H_2O and stirred constantly. After the mowiol was completely dissolved, 30 ml of glycerol and 2.25 g of N-propyl gallate were added. The solution was centrifuged for 15 minutes at 173000 rpm and aliquots were stored at -20°C.

5 M NaCl (500 ml)
146,1 g of NaCl were dissolved in 500 ml of Millipore-H2O. The solution was autoclaved and stored at room temperature.

1x PBS (1 l)
9.55 g of 10x PBS buffer (10x Dulbecco's-powder) were dissolved in 1 l of Millipore-H_2O. Solution was autoclaved and stored at room temperature.

1x PBS/DEPC (1 l)
9.55 g of 10x PBS buffer (10x Dulbecco's-powder) were dissolved in 1 l of Millipore-H_2O. 1 ml of DEPC was added and the mixture was stirred until the DEPC was completely dissolved. Solution was autoclaved and stored at room temperature.

3.7% PFA in PBS (200 ml) – prepare solution under ventilated fume hood
7.4 g of PFA were added to 100 ml of PBS. 2 drops of 10 N NaOH were added and the mixture was placed on a hotplate (60°C) and stirred until PFA was completely dissolved. 100 ml of PBS were added and the pH was adjusted to 7.3. Aliquots were frozen at -20°C.

3.7% PFA in PBS/DEPC (200 ml)
As described above, but instead of PBS, PBS/DEPC was used.

20% (w/v) SDS (100 ml) – prepare solution under ventilated fume hood
20 g of SDS were dissolved in 80 ml of Millipore-H_2O. The volume was adjusted to 100 ml. Solution was stored at room temperature.

10x TBST (1 l)
0.5 M tris, 1.5 M NaCl, 0.5% (v/v) Tween 20
60.57 g of tris and 87.66 g of NaCl were dissolved in 800 ml of Millipore-H_2O. The pH was adjusted to 7.4 with HCl. The solution was filled up with Millipore-H_2O to a volume of 1 l and filter-sterilized. 5 ml Tween 20 were added. Solution was stored at room temperature.

1 M Tris (500 ml)
60.6 g of tris were dissolved in 400 ml of Millipore-H_2O. The desired pH was adjusted with HCl and the solution was filled up with Millipore-H_2O to 500 ml. The solution was autoclaved and stored at room temperature.
For **RNase-free Tris buffer**, DEPC-H_2O was used instead of Millipore-H_2O.

4.1.10.2 DNA buffers

6x DNA loading buffer (10 ml)
30% (v/v) glycerol, 5 mM EDTA, 0.25% (w/v) bromophenol blue
3 ml of glycerol and 1 ml of 0.5 M EDTA were added to 6 ml of Millipore-H_2O. 25 mg of bromophenol blue were added. Aliquots were stored at -20°C.

10x TBE buffer (1 l)
890 mM tris, 890 mM boric acid, 20 mM EDTA
108 g of tris, 55 g of boric acid and 40 ml of 0.5 M EDTA were dissolved in 800 ml of Millipore-H_2O. The volume was then adjusted to 1 l. Solution was stored at room temperature.

Lysis buffer for mouse biopsies (100 ml)
50 mM EDTA, 50 mM tris, 0.5 % (w/v) SDS
10 ml of 0.5 M EDTA pH 8.0 and 5 ml of 1 M tris pH 8.0 were added to 97.5 ml of Milipore-H_2O. After autoclaving the solution, 2.5 ml of 20% SDS were added. Solution was stored at room temperature.

4.1.10.3 *In situ* hybridization buffers

Blocking reagent (100 ml)
10% (w/v) blocking reagent in maleic acid buffer (MAB)
10 g of blocking reagent were added to 100 ml of maleic acid buffer (MAB). While stirring, the solution was heated on a hot plate (60°C) until the blocking reagent was completely dissolved. The solution was autoclaved and aliquots were frozen at -20°C.

Hybridization buffer (10 ml)
50% deionized formamide, 1.5 x SSC, 5 mM EDTA, 0.5% CHAPS, 0.1 mg/ml heparin, 0.2% Tween 20
5 ml of deionized formamide, 750 µl of 20x SSC, 100 µl of 0.5 M EDTA, 500 µl 10% CHAPS, 10 µl of 100 mg/ml heparin, 20 µl Tween 20 were added to 3,7 ml of DEPC-H_2O. Aliquots were frozen at -20°C.

200 mM Levamisole (50 ml)
2.4 g of levamisole were dissolved in 50 ml of Millipore-H_2O. Aliquots were frozen at -20°C.

Maleic acid buffer (MAB) (500 ml)

100 mM maleic acid, 150 mM NaCl, pH 7.5

5.8 g of maleic acid and 4.4 g of NaCl were dissolved in 400 ml of Millipore-H_2O. The pH was adjusted to 7.5 with NaOH pellets and the solution was filled up with Millipore-H2O to a volume of 500 ml. Solution was autoclaved and stored at 4°C.

Maleic acid buffer with 0.1 % (v/v) Tween 20 (MABT)

500 µl of Tween 20 were added to 500 ml of maleic acid buffer. Solution was stored at 4°C.

NTE buffer (1 l)

0.5 M NaCl, 10 mM tris pH 7.5, 5 mM EDTA pH 8

100 ml of 5 M NaCl, 10 ml of 1 M tris pH 7.5 and 10 ml of 0.5 M EDTA were added to 880 ml of Millipore-H_2O. The solution was stored at 4°C.

NTMT buffer (1 l)

100 mM NaCl, 50 mM $MgCl_2$, 100 mM tris pH 9.5, 0.1 % (v/v) Tween 20

20 ml of 5 M NaCl, 50 ml of 1 M $MgCl_2$ and 100 ml 1 M tris pH 9.5 were added to 830 ml of Millipore-H_2O. 1 ml of Tween 20 was added. The solution was stored at 4°C.

10 mg/ml Proteinase K

10 mg of proteinase K were dissolved in 1 ml of proteinase K buffer. Aliquots were frozen at -20°C.

20x SSC (1 l)

3 M NaCl, 0.3 M sodium citrate tribasic dihydrate

175.3 g of NaCl and 88.2 g of sodium citrate tribasic dihydrate were dissolved in 800 ml of Millipore-H_2O. The pH was adjusted to 5 with 1 M citric acid. The solution was filled up to 1 l with Millipore-H_2O and 1 ml of DEPC was added. The solution was stirred until the DEPC was fully dissolved and autoclaved. Solution was stored at room temperature.

TE buffer (Proteinase K buffer) (1 l)

20 mM RNase-free tris pH 7.5, 1 mM EDTA/DEPC pH8

20 ml of 1 M RNase-free tris pH 7.5 and 2 ml of 0.5 M EDTA/DEPC pH 8 were added to 978 ml of DEPC-H_2O. The solution was stored at room temperature.

Tris/Glycine buffer (1 l)
100 mM tris, 100mM glycine
12.1 g of tris and 7.5 g of glycine were dissolved in 1 l of DEPC-H_2O. The solution was autoclaved and stored at room temperature.

100 mg/ml tRNA
100 mg of t-RNA were dissolved in 1 ml of DEPC-H_2O. Aliquots were frozen at -20°C.

4.1.10.4 Protein buffers

10% (w/v) Ammonium persulfate (APS) (10 ml)
1 g of ammonium persulfate was dissolved in 10 ml of Millipore-H_2O. Working aliquots were frozen at -20°C.

10x Blotting buffer (1 l) – without methanol
250 M tris, 1.92 M glycine
30.3 g of tris and 144.1 g of glycine were dissolved in 800 ml of Millipore-H_2O. The volume was then adjusted to 1 l. Solution was stored at 4°C.
To prepare **1x Blotting buffer with 10% (v/v) methanol,** 100 ml of 10x blotting buffer was mixed with 100 ml of methanol. Millipore-H_2O was added to a volume of 1 l.

5% (w/v) Milk-blocking solution (1 l)
50 g of nonfat dry milk powder was dissolved in 1l of TBST. 50 ml-aliquots were frozen at -20°C.

Ponceau-Red solution (1 l)
0.1 % (w/v) ponceau-S, 5 % (v/v) acetic acid
1 g of ponceau-S and 50 ml of acetic acid were added to 950 ml of Millipore-H_2O. Solution was stored at room temperature.

Protein loading buffer (100 ml)
60 mM tris-HCl pH 6.8, 10 % (v/v) glycerol, 3 % (w/v) SDS, 5 % (v/v) beta-mercaptoethanol, 0.005% (w/v) bromophenol blue
6 ml of 1 M tris-HCL pH 6.8, 10 ml of glycerol, 15 ml of 20 % SDS, 5 ml of beta-mercaptoethanol and 50 µl of 1 % bromophenol blue were added to 64 ml of Millipore-H_2O. Aliquots were frozen at -20°C.

10x SDS-PAGE running buffer (1 l)

250 mM tris, 1.92 M glycine, 1 % (w/v) SDS

30.3 g of tris and 144 g of glycine were dissolved in 850 ml of Millipore-H_2O by stirring. 50 ml of 20 % SDS were added and the volume was adjusted to 1 l. Solution was stored at room temperature.

The pH of the 10x solution should be 8.8, the pH of the 1x solution 8.3. Do not adjust the pH.

4.2 Methods

4.2.1 Cell culture methods

4.2.1.1 Poly-d-lysine coating

5 mg of lyophilized poly-d-lysine was reconstituted in 5 ml of sterile Millipore-H_2O to reach a concentration of 1 mg/ml. Aliquots were frozen at -20°C.
Sterile glass cover slips and glass-bottom dishes, respectively, were coated with 10 µg/ml poly-d-lysine diluted in sterile Millipore-H_2O over night at 4°C and afterwards washed three times with PBS.

4.2.1.2 Isolation of primary mouse cortical neurons

Timed-pregnant mice were sacrificed by cervical dislocation and swabbed with 70% of ethanol. The uterus was dissected and placed into a Petri dish with sterile PBS. Embryos were isolated from the uterus and the embryonic sac and transferred into a new Petri dish with sterile PBS.
Due to heterozygous parental mice, the genotype of each embryo had to be determined. For this reason, two of the limbs were collected and the identification number of each embryo was matched with its biopsy. The genotype was eventually assigned by PCR as described in 4.2.6.4.
After decapitating the embryo, the brain was isolated and placed into a 6 cm dish. Under a dissection microscope (*Leica*, MS5) the meninges was removed with fine forceps. The cerebral cortex was dissected and transferred into a 1.5 ml reaction tube with 500 µl of cortical neuron culture medium. The tissue was mechanically homogenized by pipetting it gently up and down with a fire polished Pasteur pipette. The cell suspension was then transferred into a 15 ml conical tube containing 2 ml of culture medium. The cell count was defined with a Hemocytometer (Neubauer Improved, 0.1 mm depth, 0,0025 mm^2, Precicolor, HBG Germany). 1.5 x 10^5 cells per cm^2 were seeded in culture medium onto poly-d-lysine coated wells or glass cover slips. Cells were cultured at 37°C and an atmosphere of 5% CO_2.

<u>Cortical neuron culture medium:</u>
Neurobasal medium containing:
1 x B-27 supplement
2 mM l-glutamine
50 U penicillin
50 µg/ml streptomycin

4.2.2 Nucleic acid analyses

4.2.2.1 DNA Isolation from mouse biopsies

Mouse biopsies were lysed in 190 µl of lysis buffer supplemented with 1 mg/ml of proteinase K overnight at 54°C. The next day, following addition of 250 µl lysis buffer, 250 µl of saturated NaCl was added to each sample. After 5 minutes of incubation at room temperature the samples were centrifuged for 15 min at 14000 rpm and room temperature. The supernatant was transferred into a fresh reaction tube. For DNA precipitation, 600 µl of 2-Propanol was added to the supernatant and the samples were incubated for 5 minutes. After 15 minutes of centrifugation at 14000 rpm and room temperature, the DNA pellet was washed twice with 70% of ethanol and once with 100% of ethanol. Finally the pellet was air-dried and resuspended in 50 -100 µl of sterile water (depending on the pellet size).

4.2.2.2 RNA Isolation from cells and tissues

For RNA isolation from mouse tissue, mice were sacrificed by cervical dislocation and organs of interest were immediately dissected, transferred into 2 ml reaction tubes and shock-frozen in liquid nitrogen. 50-100 mg of tissue was homogenized in 1 ml of TRIzol® using the TissueRuptor from Qiagen (Cat. No.: 9001272).

To isolate RNA from adherent cells in culture, cells were grown in a 25 cm^2 cell culture flask until reaching 80% of confluency. The culture medium was removed and 1 ml of TRIzol® was immediately added. The cell suspension was transferred into a 1.5 ml reaction tube.

Either tissue- or cell- lysates were incubated for 5 minutes at room temperature. 100 µl of BCP was added and samples were vigorously vortexed for 15 seconds. After 3 minutes of incubation at room temperature, phase separation was carried out by centrifuging the samples for 15 minutes at 12000 rpm and 4°C (Eppendorf centrifuge 5417R). The RNA-containing upper aqueous phase was transferred into a new 1.5 ml reaction tube and RNA was precipitated by adding 500 µl of isopropanol. Samples were incubated for 10 minutes at room temperature and afterwards centrifuged for 10 minutes at 12000 rpm and 4°C. The supernatant was removed and the RNA-pellet washed with 1 ml of 75% ethanol diluted with DEPC-H_2O. Samples were centrifuged for 5 minutes at 7500 rpm at 4°C and the pellet of each sample was washed again. The RNA pellets were finally air-dried and dissolved in 50-100 µl of DEPC-treated water by passing it a few times through a pipette tip. RNA was either used directly for cDNA-synthesis or frozen at -80°C.

4.2.2.3 RNA concentration measurement

5 µl of RNA was diluted into 195 µl of DEPC-treated water (1:40 dilution) and transferred into a quartz cuvette (light path 10 mm, Hellma 105.202-Qs,). The optical density (OD) at wavelengths of 260 nm (OD_{260}) and 280 nm (OD_{280}), respectively, was measured using a spectrophotometer (GE Healthcare, Gene Quant 1300). DEPC-treated water was used as reference. An OD_{260} = 1 corresponds to a RNA concentration of 40 µg/ml. The OD_{260}/OD_{280} should be between 1.8 and 2. Lower concentrations indicate contamination with proteins.

4.2.2.4 cDNA-Synthesis

cDNA was generated by reverse-transcription (RT) from total RNA, using the QuantiTect Reverse Transcription Kit (Qiagen). For each reaction 1 µg of total RNA was incubated with 2 µl of 7x gDNA Wipeout Buffer and 11 µl of Rnase-free water at 42°C for 3.5 minutes. Reverse transcription was then carried out by adding 6 µl of reverse-transcription master mix (4 µl 5x Quantiscript RT Buffer, 1 µl RT Primer Mix, 1 µl Quantiscript Reverse Transcriptase) to the entire genomic DNA elimination reaction, followed by incubation at 42°C for 15 minutes, then 95°C for 3 minutes. cDNA was stored at -20°C.

4.2.2.5 Polymerase chain reaction (PCR)

Each PCR was carried out in a 30 µl-reaction mix containing 1x reaction buffer with 1.5 mM $MgCl_2$ (Genecraft), 250 µM of each dNTP (Genecraft), 0.1 µM of each forward and reverse primer and 1.5 units of Taq polymerase (Genecraft). As template either 2 µl of cDNA (see 4.2.2.4) or 2 µl of a 1:40 dilution of isolated DNA was used (see 4.2.2.1).

DNA amplification was accomplished in an Eppendorf thermocycler (Eppendorf Mastercycler) with an initial denaturation step for 3 minutes at 94°C, followed by 20-40 repeated cycles of 30 seconds denaturation at 94°C, 30 seconds annealing at 50-60°C (depending on primers) and 1 minute elongation at 72°C. Additionally a final elongation step for 10 minutes at 72°C was applied. The specific annealing temperature for each primer set is listed in 4.1.8.

4.2.2.6 Agarose gel electrophoresis

For agarose gel electrophoresis the Bio-Rad Mini-Sub GT Cell system was used. Electrophoresis modules were assembled according to the manufacturer's instructions.

An appropriate amount of agarose was added to 0.5x TAE buffer in a microwavable bottle to obtain a final concentration of 1-1.7%. The agarose was boiled in a microwave (Siemens) until it was completely dissolved and allowed to cool down to around 60°C before 0.5 µg/ml ethidiumbromide was added. The molten agarose was cast on the removable UV-transparent plastic tray with the aid of a gel caster. Combs with 8 or 15 wells and 0.75 mm thickness were positioned into the appropriate slots of the tray. After the agarose solution had become solid, the combs were removed and the gel-tray was placed on the stage of the Mini Sub-cell base. The gel was submerged with 0.5x TAE buffer. A molecular weight marker (5-7 µl/ well) and DNA samples (15-30 µl/ well) with an appropriate amount of 6x gel loading buffer were loaded into the wells. Electrophoresis was conducted at 90 V for 30-40 minutes with a powerpac 300 power supply from Bio-Rad. DNA fragments were visualized under a UV transilluminator (PeqLab) and photographs were taken with an image analysis system from PeqLab.

4.2.2.7 Real-time PCR

Real-time PCR analysis was performed with the LightCycler 480 (Roche), in LightCycler 480 multiwell 96 plates (Roche). Each 20 µl/well reaction included 10 µl Lightcycler 480 SYBR Green I Master (Roche), 0.5 µM of each forward and reverse primer and 5 ng cDNA. Following Taq activation and initial denaturation at 95°C for 5 minutes, the amplification and quantification was performed for 40 cycles with 15 seconds denaturation at 95°C and 15 seconds annealing/elongation at 59°C. Fluorescence readings were taken after each cycle. At the end of each experiment a melting curve analysis was performed to determine the specificity of the amplification (50-95°C with a heating rate of 5 acquisitions per °C and a continuous measurement). The crossing point (CP) that is defined as the point at which the measured fluorescence rises above background fluorescence was determined automatically using the second derivative maximum mode of the LightCycler Software.

The relative amount of target mRNA normalized to *beta-microgobulin* gene was calculated according to Pfaffl, 2001. Each reaction was performed in duplicate.

All oligonucleotides used in this experiment were designed using AiO software (Karreman, C, 2002). Primers were designed to span at least one intron of the genomic sequence.

4.2.2.8 Generation of DIG-labeled RNA probes

Antisense riboprobes were generated from the pcDNA3-m-Spir-2-NT plasmid template for the mouse *spir-2* gene and from the pcDNA3-Myc-Spir-1-CT plasmid template for the *spir-1* gene (Kerkhoff et al., 2001; Pleiser et al., 2011).
The plasmids were linearized by restriction digestion. Each 50 µl reaction included 5 µl of the appropriate restriction buffer, 4 µl of the *Bam*HI restriction enzyme (stock: 20.000 U/ml) and 5 µg of the plasmid. The reactions were incubated for 1.15 hours at 37 °C and afterwards purified using the NucleoSpin Kit according to the manufacturers instructions. The DNA concentration was measured and 1 µg of the linearized and purified template was used to generate the DIG labeled antisense RNA probes. This *in vitro* transcription was conducted with the DIG RNA labeling Kit from Roche using the Sp6 polymerase according to the manufacturers instructions. The DIG-labeled RNA probes were finally precipitated with lithium chloride. 2.5 µl of 4 M lithium chloride and 75 µl of ice-cold ethanol were added to the entire *in vitro* transcription reaction. The samples were incubated for 4.5 hours at -20°C and centrifuged for 15 minutes at 13000 rpm and 4°C. The probes were washed twice with 70% of ethanol, air-dried, resuspended in 20 µl of DEPC-H_2O and stored at -20°C.

4.2.2.9 *In situ* hybridization

For *in situ* hybridizations, paraffin sections from CD1 mouse embryos and adult mouse tissues were prepared as described in 4.2.5.1. Some paraffin embedded sections were kindly provided from Prof. Dr. Manfred Gessler, University of Würzburg.
The sections were dewaxed two times for 10 minutes in xylol and rehydrated in a graded ethanol series (5 minutes in 100% ethanol, 5 minutes in 95% ethanol, 5 minutes in 70% ethanol, 5 minutes at 50% ethanol), followed by a short incubation in DEPC-H_2O.

<u>Prehybridization</u>
The sections were incubated as follows:

2x 5 minutes with PBS/DEPC
2x 5 minutes with PBS/DEPC containing 100mM glycine
15 minutes with PBS/DEPC containing 0.3 % Triton X-100
2x 5 minutes with PBS/DEPC

The sections were then permeabilized for 30 minutes with TE buffer, containing 10 µg/ml proteinase K, shortly washed with PBS/DEPC and postfixed for 5 minutes with

3.7% paraformaldehyde in PBS/DEPC at 4°C. After washing with PBS/DEPC, the sections were incubated for 1-3 hours with prehybridization buffer (4x SSC, containing 50% deionized formamide) at 37°C. 1.65 µl of t-RNA (100 mg/ml) and 15 µl of the DIG-labeled RNA probe were added to 1.5 ml of hybridization buffer. The hybridization mix was boiled for 3 minutes at 95°C and finally each section was overlaid with 60 µl of hybridization mix, covered with *Parafilm* and incubated over night at 60°C in a humid chamber.

Posthybridization (not necessary to work RNase free)

The following day, slides were immersed for 5 minutes in 2x SSC to remove the *Parafilm* and washed as follows:

3 x 20 min with 2x SSC at room temperature
40 min with 0.5x SSC/20% formamide at 50°C
20 min with 0.5x SSC/20% formamide at 37°C

To digest any single-stranded RNA, sections were first incubated for 15 minutes with NTE buffer at 37°C and then for 30 minutes with NTE buffer containing 20 µg/ml RNase A at 37°C.

Sections were washed again as follows:

30 min with 0.5x SSC/20% formamide at 50°C
30 min with 2x SSC at room temperature

Immunological detection

Sections were incubated for 1 hour with 1% blocking reagent in MABT buffer at room temperature. An alkaline phosphatase conjugated anti-digoxigenin antibody, 1:5000 dilution with 1% blocking reagent in MABT buffer, was applied over night at 4°C. The following day sections were washed as follows:

4x 5 minutes with TBST
3x 15 minutes with TBST
2x 10 minutes with NTMT
1x 10 minutes with NTMT + 2 mM levamisole

Alkaline phosphatase activity was revealed by incubating the sections with BM purple solution from Roche. BM purple was centrifuged for 5 minutes at 3000 rpm and room temperature and 2 mM levamisole were added to the supernatant. The sections were incubated with that solution for 1 to 7 days. When color development has completed, sections were washed two times for 15 minutes with NTMT buffer, one time for 10 minutes with PBS and shortly with Millipore-H_2O. Sections were finally embedded in mowiol solution.

4.2.3 Protein analyses

4.2.3.1 Preparation of whole protein lysates

For protein lysates from adherent cells in culture, cells were grown in 6-well cell culture dish. The culture medium was removed and cells were washed 2 times with PBS. 200 µl of protein sample buffer were added to the well and lysed cells were scraped off with a pipette tip and transferred into a 1.5 ml reaction tube.

4.2.3.2 SDS polyacrylamide gel electrophoresis (SDS-PAGE)

SDS-PAGE was carried out using the Mini-PROTEAN 3 system from Bio-Rad (Cat. No.: 165-3301). Glass cassettes and electrophoresis modules were assembled according to the manufacturer's instructions. A resolving gel (7% acrylamide) was prepared and poured between the vertical assembled glass cassettes. An approximately 1 cm gap was left for the stacking gel. The solution was overlaid with isopropanol. After the gel had polymerized, isopropanol was removed and the gel surface was rinsed with distilled water. A stacking gel (4% acrylamide) was prepared and poured onto the resolving gel until the shorter glass plate was reached. A comb with 10 wells was inserted and the gel was allowed to polymerize. The gel cassette was placed into the electrophoresis module and the tank was filled with 1x SDS-PAGE running buffer. The comb was removed and wells were thoroughly rinsed with 1x SDS-PAGE running buffer. Protein samples (see 4.2.3.1) were boiled at 95°C for 5 minutes and shortly centrifuged. A molecular weight marker (7 µl/ well) and protein samples (20 µl/ well) were loaded into the wells. Electrophoreses was conducted at 60 mA (in case two gels were run) with a powerpac 300 power supply (Bio-Rad) for approximately 1 hour. After electrophoresis had completed, the gel was removed by separating the two glass plates of the gel cassette and subjected to Western blotting.

<u>Resolving gel (7%) (10 ml):</u>
5 ml H_2O
2.5 ml 1.5 M tris pH 8.8
50 µl 20% SDS
2.3 ml acrylamide (30%)/ bisacrylamide (0,8%) (37.5:1)
100 µl APS
4 4 µl TEMED

Stacking gel (4%) (5ml):
3 ml H_2O
1.25 ml 0.5 M tris pH 6.8
25 µl 20% SDS
670 µl acrylamide (30%)/ bisacrylamide (0,8%) (37.5:1)
40 µl 10% APS
4 µl TEMED

4.2.3.3 Western Blot

For Western blotting the Mini Trans-Blot Cell system from Bio-Rad (Cat. No.: 170-3930) was used. Blotting modules were assembled according to the manufactures instructions. A 0,45 µm nitrocellulose membrane and 2 Whatman filters were cut to the dimension of the gel. Fiber pads, Whatman filters and the membrane were soaked in 1x blotting buffer for 10 minutes. The gel sandwich was then prepared in following order: fiber pad, 1 sheet of Whatman filter, gel, nitrocellulose membrane, 1 sheet of Whatman filter, fiber pad. This sandwich was placed onto the cathode side (black) of the gel-holder cassette and air-bubbles were removed by rolling a glass pipette over the fiber pad. The blotting cassette was closed, locked and placed with the electrode assembly into the buffer tank. The tank was then completely filled with 1x blotting buffer and electro-blotting was conducted at 150 mA for 2 hours with a powerpac 300 power supply from Bio-Rad. Upon completion of the run, the blotting modules were disassembled and the membrane was stained with Ponceau Red to verify the loading control. After destaining the membrane with Millipore-H_2O, unspecific binding sites of the membrane were blocked with 5% non-fat milk in 1x TBST over night at 4°C.

4.2.3.4 Immunodetection

Proteins were probed with a primary anti-Spir-1 antibody (SA3233), diluted 1:1000 in TBST, for either 3 hours at room temperature or overnight at 4°C.
After incubation, the membrane was washed 3 times with TBST for 10 minutes and then a peroxidase conjugated secondary antibody, diluted 1:5000 in TBST, was applied for 1 hour. After washing the membrane 3 times for 10 minutes with TBST, protein detection was carried out by ECL chemiluminescence reaction. The membrane was incubated for 2-3 min in a 1:1 mixture of ECL solutions 1 and 2. Signals were finally visualised by exposure of the membrane to an X-ray film, which was subsequently developed with a film- developing device from Kodak.

4.2.4 Immunocytochemistry

Immunocytochemistry was performed with primary cortical neurons seeded on poly-d-lysine coated glass cover slips in 24-well plates (300.000 cells/well).
Cells were fixed with 3.7% paraformaldehyde for 20 minutes at 4˚C and incubated for 30 min with 0.3% Triton X-100, 3% donkey serum and 1% BSA in phosphate buffered saline (PBS). A primary Map-2 antibody (4.8 µg/ml) was applied over night in PBS with 0.3% Triton X-100, 3% donkey serum and 1% BSA. After washing the cells three times with PBS, a secondary donkey anti-mouse antibody, diluted 1:200 in PBS with 0.3% Triton X-100, 3% donkey serum and 1% BSA, was applied for 1.5 hours at room temperature. Cells were washed three times and mounted in mowiol solution. Immunofluorescence was analyzed with a *Leica AF6000LX imaging system*, equipped with a *Leica* HCX PL APO 63x/1.30 glycerol objective and a *Leica* DFC350FX camera.

4.2.5 Histology

For the preparation of either cryostat or paraffin sections of adult mouse tissues, mice (25-30 g) were first anesthetized with a mixture of xylazine and ketamine. 0.2 ml of 2% xylazine were combined with 0.6 ml of 10% ketamine and 40 µl of that cocktail were intraperitoneally injected. After 10 minutes mice were intracardiacally perfused with first 20 ml of PBS and then with 20 ml of 3.7% paraformaldehyde. Tissues of interest were dissected and postfixed over night in 3.7% paraformaldehyde at 4°C. To prepare paraffin section of mouse embryos, timed-pregnant mice were sacrificed by cervical dislocation and embryos were isolated from the uterus and the embryonic sac and transferred into a 15 ml reaction tube containing 3.7% paraformaldehyde.

Preparation of cryostat section

Cryostat section of the adult mouse brain were prepared from *spir-1*$^{+/+}$ / *thy1*-GFP-M and *spir-1*$^{gt/gt}$ / *thy1*-GFP-M mice. After the postfixation over night in 3.7 % paraformaldehyde, the brains was washed two times with PBS and incubated in 30% sucrose/PBS solution at 4°C until they have sunk. The brains were then embedded in O.C.T embedding compound and 15 µm thick horizontal sections were cut with a *Leica* CM 1950 cryostat device. Sections were stored at -20°C.

Preparation of paraffin sections for *in situ* hybridization

After the postfixation over night in 3.7% paraformaldehyde, mouse embryos or adult mouse tissues, respectively were washed two times with DEPC-H_2O and dehydrated in a graded ethanol series (1 hour in 25% ethanol, 1 hour in 50% ethanol, 1 hour in 70% ethanol, 1 hour in 80% ethanol, 1 hour in 90% ethanol, over night in 100% ethanol). Before embedding in paraffin, tissues were incubated two times for 5 minutes with xylol and over night with a 1:2 dilution of xylol/paraffin at 60°C. The tissues were then incubated for 2-3 days in paraffin at 60°C (twice a day the paraffin was exchanged with fresh paraffin) before they were embedded in appropriate embedding molds. 6 µm thick sections were cut with a microtome from *Leica*. Sections were stored at room temperature.

5 Bibliography

Aguda, A.H., Burtnick, L.D., and Robinson, R.C. (2005). The state of the filament. EMBO Rep 6, 220-226.

Azoury, J., Lee, K.W., Georget, V., Rassinier, P., Leader, B., and Verlhac, M.H. (2008). Spindle positioning in mouse oocytes relies on a dynamic meshwork of actin filaments. Curr Biol 18, 1514-1519.

Bradke, F., and Dotti, C.G. (1999). The role of local actin instability in axon formation. Science 283, 1931-1934.

Bray, D (1973). Branching patterns of individual sympathetic neurons in culture. J Cell Biol 56, 702-712.

Canto, C.B., Wouterlood, F.G., and Witter M.P. (2008). What does the anatomical organization of the entorhinal cortex tell us? Neural Plast.

Chen, W., Feng, Y., Chen, D., and Wandinger-Ness, A. (1998). Rab11 is required for trans-golgi network-to-plasma membrane transport and a preferential target for GDP dissociation inhibitor. Mol Biol Cell 9, 3241-3257.

Chesarone, M.A., and Goode, B.L. (2009). Actin nucleation and elongation factors: mechanisms and interplay. Curr Opin Cell Biol 21, 28-37.

Chhabra, E.S., and Higgs, H.N. (2007). The many faces of actin: matching assembly factors with cellular structures. J Cell Sci 22, 1110-1121.

Ciccarelli, F.D., Borg, P., and Kerkhoff, E. (2003). The KIND module: a putative signaling domain evolved from the C lobe of the protein kinase fold. Trends Biochem Sci 28, 349-352.

Craig, A.M., and Banker, G. (1994). Neuronal polarity. Annu Rev Neurosci, 17, 267-310.

Dahlgaard, K., Raposo, A.A., Niccoli, T., and St Johnston, D. (2007). Capu and Spire assemble a cytoplasmic actin mesh that maintains microtubule organization in the Drosophila oocyte. Dev Cell 13, 539-553.

Dailey, M.E., and Smith, S.J. (1996). The dynamics of dendritic structure in developing hippocampal slices. J Neurosci 16, 2983-2994.

Dominguez, R., and Holmes, K.C. (2011). Actin structure and function. Annu Rev Biophys 40, 169-186.

Dotti, C.G., Sullivan, C.A., and Banker, G.A. (1988). The establishment of polarity by hippocampal neurons in culture. J Neurosci 8, 1454-1468.

Ehlers, M.D. (2000). Reinsertion or degradation of AMPA receptors determined by activity-dependent endocytic sorting. Neuron 28, 511-525.

Feng, G., Mellor, R.H., Bernstein, M., Keller-Peck, C., Nguyen, Q.T., Wallace, M., Nerbonne, J.M., Lichtmann, J.W., and Sanes, J.R. (2000). Imaging neuronal subsets in transgenic mice expressing multiple spectral variants of GFP. Neuron 28, 31-51.

Fujii, T., Iwane, A.H., Yanagida, T., and Namba, K. (2010). Direct visualization of secondary structures of F-actin by electron microscopy. Nature 467, 724-728.

Higgs, H.N. (2005). Formin proteins: a domain-based approach. Trends Biochem Sci 30, 342-353.

Hurley, J.H. (2006). Membrane binding domains. Biochim Biophys Acta 1761, 805-811.

Kaech, S., and Banker, G. (2006). Culturing hippocampal neurons. Nat Protoc 1, 2406-2415.

Karreman, C. (2002). AiO, combining DNA/protein programs and oligo-management. Bioinformatics 18, 884-885.

Kelly, A.E., Kranitz, H., Dötsch, V., and Mullins, R.D. (2006). Actin binding to the central domain of WASP/Scar proteins plays a critical role in the activation of the Arp2/3 complex. J Biol Chem 281, 10589-10597.

Kerkhoff, E., Simpson, J.C., Leberfinger, C.B., Otto, I.M., Doerks, T., Borg, P., Rapp, U.R., Raabe, T., and Pepperkok, R. (2001). The Spir actin organizers are involved in vesicle transport processes. Curr Biol 11, 1963-1968

Kerkhoff, E. (2006). Cellular functions of the Spir actin-nucleation factors. Trends Cell Biol 16, 477-483.

Kerkhoff, E. (2011). Actin dynamics at intracellular membranes: The Spir/formin nucleator complex. Eur J Cell Biol 90, 922-925.

Kovar, D.R., Kuhn, J.R., Tichy, A.L., and Pollard, T.D. (2003). The fission yeast cytokinesis formin Cdc12p is a barbed end actin filament capping protein gated by profilin. J Cell Biol 161, 875-887.

Leader, B., Lim, H., Carabatsos, M.J., Harrington, A., Ecsedy, J., Pellman, D., Maas, R., Leder, P. (2002). Formin-2, polyploidy, hypofertility and positioning of the meiotic spindle in mouse oocytes. Nat Cell Biol 4, 921-928.

Machesky, L.M., and Insall, R.H. (1998). Scar1 and the related Wiskott-Aldrich syndrome protein, WASP, regulate the actin cytoskeleton through the Arp2/3 complex. Curr Biol 8, 1347-1256.

Manseau, L.J., and Schupbach, T. (1989). cappuccino and spire: two unique maternal-effect loci required for both the anteroposterior and dorsoventral patterns of the Drosophila embryo. Genes Dev 3, 1437-1452.

Miesenböck, G., De Angelis, D.A., and Rothmann, J.E. (1998). Visualizing secretion and synaptic transmission with pH-sensitive green fluorescent proteins. Nature 394, 192-195.

Misra, S., and Hurley, J.H. (1999). Crystal structure of a phosphatidylinositol 3-phosphate-specific membrane-targeting motif, the FYVE domain of Vps27p. Cell 97, 657-666.

Morel, E., Parton, R.G., and Gruenberg, J. (2009). Annexin A2-dependent polymerization of actin mediates endosome biogenesis. Dev Cell 16, 445-457.

Neukirchen, D., and Bradke, F. (2011). Neuronal polarization and the cytoskeleton. Semin Cell Dev Biol 22, 825-833.

Ostermeier, C., and Brunger, A.T. (1999). Structural basis of Rab effector specificity: crystal structure of the small G protein Rab3A complexed with the effector domain of rabphilin-3A. Cell 96, 363-374.

Otto, I.M., Raabe, T., Renefahrt, U.E., Borg, P., Rapp, U.R., and Kerkhoff, E. (2000). The p150-Spir protein provides a link between c-Jun N-terminal kinase function and actin reorganization. Curr Biol 10, 345-348.

Otomo, T., Tomchick, D.R., Otomo, C., Panchal, S.C., machius, M., Rosen, M.K. (2005). Structural basis of actin filament nucleation and processive capping by a formin homology 2 domain. Nature 433, 488-494.

Park, M., Penick, E.C., Edwards, J.G., Kauer, J.A., and Ehlers, M.D. (2004). Recycling endosomes supply AMPA receptors for LTP. Science 305, 1972-1975.

Park, M., Salgado, J.M., Ostroff, L., Helton, T.D., Robinson, C.G., Harris, K.M., and Ehlers, M.D. (2006). Plasticity-induced growth of dendritic spines by exocytic trafficking from recycling endosomes. Neuron 52, 817-830.

Paunola, E., Mattila, P.K., and Lappalainen, P. (2002). WH2 domain: a small, versatile adapter for actin monomers. FEBS Lett 513, 92-97.

Pechlivanis, M., Samol, A., and Kerkhoff E. (2009). Identification of a short Spir interaction sequence at the C-terminal end of formin subgroup proteins. J Biol Chem 284, 25324-25333.

Pfaffl, M.W. (2001). A new mathematical model for relative quantification in real-time RT-PCR. Nucleic Acids Res 29.

Pfender, S., Kuznetsov, V., Pleiser, S., Kerkhoff, E., and Schuh, M. (2011). Spire-type actin nucleators cooperate with Formin-2 to drive asymmetric oocyte division. Curr Biol 21, 955-960.

Pleiser, S., Rock, R., Wellmann, J., Gessler, M., and Kerkhoff E. (2010). Expression patterns of the mouse Spir-2 actin nucleator. Gene Expr Patterns 10, 345-350.

Pollard, T.D., and Beltzner, C.C (2002). Structure and function of the Arp2/3 complex. Vurr Opin Struct Biol 12, 768-774.

Pollard, T.D., and Borisy, G.G (2003). Cellular motility driven by assembly and disassembly of actin filaments. Cell 112, 453-465.

Pollard, T.D. (2007). Regulation of actin filament assembly by Arp2/3 complex and formins. Annu Rev Biophys Biomol Struct 36, 451-477.

Pollard, T.D., and Cooper, J.A. (2009). Actin, a central player in cell shape and movement. Science 326, 1208-1212.

Qualmann, B., and Kessels, M.M. (2009). New players in actin polymerization--WH2-domain-containing actin nucleators. Trends Cell Biol 19, 276-285.

Quinlan, M.E., Heuser, J.E., Kerkhoff, E., and Mullins, R.D. (2005). Drosophila Spire is an actin nucleation factor. Nature 433, 382-388

Quinlan, M.E., Hilgert, S., Bedrossian, A., Mullins, R.D., and Kerkhoff, E. (2007). Regulatory interactions between two actin nucleators, Spire and Cappuccino. J Cell Biol 179, 117-128.

Quinlan, M.E., and Kerkhoff, E. (2008). Actin nucleation: bacteria get in-Spired. Nat Cell Biol 10, 13-15

Renault, L., Bugyi, B., and Carlier, M.F. (2008). Spire and Cordon-bleu: multifunctional regulators of actin dynamics. Trends Cell Biol 18, 494-504.

Romero, S., Le Clainche, C., Didry, D., Egile, C., Pantaloni, D., and Carlier, M.F. (2004). Formin is a processive motor that required profilin to accelerate actin assembly and associated ATP hydrolysis. Cell 119, 419-429.

Rosales-Nieves, A.E., Johndrow, J.E., Keller, L.C., Magie, C.R., Pinto-Santini, D.M., and Parkhurst, S.M. (2006). Coordination of microtubule and microfilament dynamics by Drosophila Rho1, Spire and Cappuccino. Nat Cell Biol 8, 367-376.

Ryley, D.A., Wu, H.H., Leader, B., Zimon, A., Reindollar, R.H., and Gray, M.R. (2005). Characterization and mutation analysis of the human formin-2 (FMN2) gene in women with unexplained infertility. Fertil Steril 83, 1363-1371.

Schönichen, A., and Geyer, M. (2010). Fifteen formins for an actin filament: a molecular view on the regulation of human formins. Biochim Biophys Acta 1803, 152-163.

Schuh, M., and Ellenberg, J. (2008). A new model for asymmetric spindle positioning in mouse oocytes. Curr Biol 18, 1986-1992.

Schuh, M. (2011). An actin-dependent mechanism for long-range vesicle transport. Nat Cell Biol 13, 1431-1436

Schumacher, N., Borawski, J.M., Leberfinger, C.B., Gessler, M., and Kerkhoff, E. (2004). Overlapping expression pattern of the actin organizers Spir-1 and formin-2 in the developing mouse nervous system and the adult brain. Gene Expr Patterns 4, 249-255

Scott, E.K., and Luo, L. (2001). How do dendrites take their shape? Nat Neurosci 4, 359-365.

Shimada, A., Nyitrai, M., Vetter, I.R., Kühlmann, D., Bugyi, B., Narumiya, S., Geeves, M.A., and Wittinghofer, A. (2004). The core FH2 domain of diaphanous-related formins is an elongated actin binding protein that inhibits polymerization. Mol Cell 13, 511-522.

Simerly, C., Nowak, G., de Lanerolle, P., and Schatten, G. (1998). Differential expression and functions of cortical myosin IIA and IIB isotypes during meiotic maturation, fertilization, and mitosis in mouse oocytes and embryos. Mol Biol Cell 9, 2509-2525.

Sönnichsen, B., De Renzis, S., Nielsen, E., Rietdorf, J., and Zerial, M. (2000). Distinct membrane domains on endosomes in the recycling pathway visualized by multicolor imaging of Rab4, Rab5, and Rab11. J Cell Biol 149, 901-914.

Stappenbeck, T.S., Wong, M.H., Saam, J.R., Mysorekar, I.U., and Gordon, J.I. (1998). Notes from some crypt watchers: regulation of renewal in the mouse intestinal epithelium. Curr Opin Cell Biol 10, 702-709.

Stenmark, H., Aasland, R., Toh, B.H., and D'Arrigo, A. (1996). Endosomal localization of the autoantigen EEA1 is mediated by a zinc-binding FYVE finger. J Biol Chem 271, 24048-24054.

Tahirovic, S., and Bradke, F. (2009). Neuronal polarity. Cold Spring Harb Perspect Biol 1.

Vavylonis, D., Kovar, D.R., O'Shaughnessy, B., and Pollard, T.D. (2006). Model of formin-associated actin filament elongation. Mol Cell 21, 455-466.

Vizcarra, C.L., Kreutz, B., Rodal, A.A., Toms, A.V., Lu, J., Zheng, W., Quinlan, M.E., and Eck, M.J. (2011). Structure and function of the interacting domains of Spire and Fmn-familiy formins. Proc Natl Acad Sci U S A, 108, 11884-11889.

Wang, Z., Edwards, J.G., Riley, N., Provance, D.W. Jr., Karcher, R., Li, X.D., Davison, I.G., Ikebe, M., Mercer, J.A., Kauer, J.A., Ehlers, M.D (2008). Myosin Vb mobilizes recycling endosomes and AMPA receptors for postsynaptic plasticity. Cell 135, 535-548.

Wellington, A., Emmons, S., James, B., Calley, J., Grover, M., Tolias, P., and Manseau, L. (1999). Spire contains actin binding domains and is related to ascidian posterior end mark-5. Development 126, 5267-5274.

Witke, W. (2004). The role of profilin complexes in cell motility and other cellular processes. Trends Cell Biol 14, 461-469.

Witte, H., Neukirchen, D., and Bradke, F. (2008). Microtubule stabilization specifies initial neuronal polarization. J Cell Biol 180, 619-632.

Xu, Y., Moseley, J.B., Sagot, I., Poy, F., Pellman, D., Goode, B.L., and Eck, M.J. (2004). Crystal structures of a Formin Homology-2 domain reveal a tethered dimer architecture. Cell 116, 711-723.

Zeth, K., Pechlivanis, M., Samol, A., Pleiser S., Vonrhein, C., and Kerkhoff E. (2011). Molecular basis of actin nucleation factor cooperativity: crystal structure of the Spir-1 kinase non-catalytic C-lobe domain (KIND)*formin-2 SPIR interaction motif (FSI) complex. J Biol Chem 286, 30732-30739.

6 Appendix

6.1 List of abbreviations

°C	Degree Celsius
µg	Microgram
APS	Ammoniumpersulfate
BCP	1-bromo-3-chloropropane
bp	Basepairs
BSA	Bovine Serum Albumin
Cat. No.	Catalog Number
CHAPS	3- [(3-Cholamidopropyl)dimethyl-ammonio]-1-propanesulfonate
CO_2	Carbon dioxide
DAPI	4',6-Diamidino-2-phenylindol
dATP	Deoxyadenosine triphosphate
dCTP	Deoxycytidine triphosphate
dGTP	Deoxyguanosine triphosphate
DNA	Deoxyribonucleic acid
dNTP	Desoxynucleosidtriphosphate
dTTP	Deoxythymidine triphosphate
ECL	Enhanced Chemiluminescence
EDTA	Ethylenediaminetetraacetic acid
et al.	Et alii
FITC	Fluorescein isothiocyanate
g	Gram
HBSS	Hank's buffered Salt Solution
HCl	Hydrochloric acid
kDa	Kilo dalton
ko	Knock-out
LiCl	Lithium chloride
mg	Milligram
min	Minutes
mM	Millimolar
NaOH	Sodium hydroxide
OD	Optical density
PAGE	Polyacrylamide Gel Electrophoresis
PBS	Phosphate buffered saline
PFA	Paraformaldehyde

rpm	Rounds per minute
SDS	Sodium dodecylsulfate
TAE	Tris-Acetate-EDTA
TEMED	N,N,N',N'-Tetramethylethylenediamine
TBS	Tris buffered saline
Tris	Tris(hydroxymethyl)aminomethane
TRITC	Tetramethylrhodamine isothiocyanate
V	Volt
v/v	Volume/Volume
w/v	Weight/Volume
wt	Wildtype

6.2 Acknowledgements

I would like to express my sincere gratitude to my supervisor Prof. Dr. Eugen Kerkhoff for giving me the opportunity to work on this fantastic project. I am grateful for his excellent support and trust throughout the years and for helping me whenever I needed his assistance.

I would also like to thank Prof. Dr. Ulrich Bogdahn for the possibility to work in his institute.

I am very grateful to Prof. Dr. Thomas Raabe for being my second supervisor.

I want to thank Manfred Gessler and his group for sharing protocols and providing materials for *in situ* hybridization analyses.

Special thank goes to all of my colleagues and former members of the group for creating such a wonderful working environment. During the years you all have become my friends and it is a great pleasure to know every single one of you. Thank you Sabine, Agnes, Annette, Susanne, Tanja, Isabell and Markos for helping me, listening to me, supporting and inspiring me in any situation- you are awesome!

I am very grateful to Dr. Thilo Spruss and Engelbert Meier for their outstanding help within the animal facility.

I want to express my deepest gratitude to Nadine, Judith, Katharina, and Anya for constantly encouraging and supporting me and just being the most wonderful friends in the world!!!

Thank you Ema for the fantastic time and for everything you have done for me.

Simon, I want to thank you for your strong mental support during the last period of my thesis, for listening to me whenever I had a problem, for your solidarity and patience.

My sincerest gratitude goes to my parents Hannelore and Klaus and my brother Carsten, for their constant love, trust, and mental support that made this work possible!

6.4 List of publications

Zeth, K., Pechlivanis, M., Samol, A., **Pleiser S**., Vonrhein, C., and Kerkhoff E. (2011). Molecular basis of actin nucleation factor cooperativity: crystal structure of the Spir-1 kinase non-catalytic C-lobe domain (KIND)*formin-2 SPIR interaction motif (FSI) complex. J Biol Chem 286, 30732-30739.

Pfender, S., Kuznetsov, V., **Pleiser, S**., Kerkhoff, E., and Schuh, M. (2011). Spire-type actin nucleators cooperate with Formin-2 to drive asymmetric oocyte division. Curr Biol 21, 955-960.

Pleiser, S., Rock, R., Wellmann, J., Gessler, M., and Kerkhoff E. (2010). Expression patterns of the mouse Spir-2 actin nucleator. Gene Expr Patterns 10, 345-350.

Camarero, G., Tyrsin, O.Y., Xiang, C., Pfeiffer, V., **Pleiser, S**., Wiese, S., Götz, R., Rapp, U.R (2006). Mol Cell Biol 26, 7103-7115.